Nonlinear dispersion properties of one-dimensional mechanical metamaterials with inertia amplification

note finali coverpage

(Article begins on next page)

13 July 2024

This is a post-peer-review, pre-copyedit version of the paper

Nonlinear dispersion properties of one-dimensional mechanical metamaterials with inertia amplification

by Valeria Settimi[1]*, Marco Lepidi[2], Andrea Bacigalupo[2]

[1] *Department of Civil and Building Engineering and Architecture, Polytechnic University of Marche, Ancona, Italy*
[2] *Department of Civil, Chemical and Environmental Engineering, University of Genoa, Genoa, Italy*

*Corresponding author: v.settimi@staff.univpm.it

Please cite this work as follows:

Publisher link and Copyright information:

Nonlinear dispersion properties of one-dimensional mechanical metamaterials with inertia amplification

Valeria Settimi[a,*], Marco Lepidi[b], Andrea Bacigalupo[b,]

[a] *DICEA - Dipartimento di Ingegneria Civile, Edile e Architettura, Università Politecnica delle Marche, Ancona (Italy)*
[b] *DICCA - Dipartimento di Ingegneria Civile, Chimica e Ambientale, Università di Genova, Genova (Italy)*

Abstract

Architected metamaterials offering superior dynamic performances can be conceived by inducing local mechanisms of inertia amplification in the periodic microstructure. A one-dimensional cellular lattice characterized by a pantograph mechanism in the tetra-atomic cell is proposed as minimal physical realization of inertially amplified metamaterial. A discrete model is formulated to describe the undamped free dynamics of the cell microstructure. The ordinary differential equations of motion feature quadratic and cubic inertial nonlinearities, induced by the indeformability of the pantograph arms connecting the principal atoms with the secondary atoms, serving as inertial amplifiers. An asymptotic approach is employed to analytically determine the dispersion properties governing the free propagation of harmonic waves in the pantographic metamaterial. First, the linear wavefrequencies and waveforms are obtained by solving the eigenproblem governing the lowest asymptotic order. An invariant parametric form is achieved for the pass and stop band structure, corresponding to propagation and attenuation branches of the dispersion spectrum in the plane of complex wavenumbers. The major effects due to the mass ratio of the inertial amplifiers are discussed. Particularly, the existence conditions, amplitude and centerfrequency of the band gap separating the acoustic and optical pass bands are determined analytically. Second, the nonlinear wavefrequencies and waveforms are obtained by solving the hierarchical linear problems governing the higher asymptotic orders. Analytical, although asymptotically approximate, functions are achieved for the nonlinear wavefrequencies and waveforms, which show quadratic dependence on the oscillation amplitudes. The mechanical conditions for the softening/hardening behaviour of the nonlinear wavefrequencies and the different topological properties of the invariant manifolds associated to the nonlinear waveforms are discussed. Finally, numerical simulations are provided to validate the analytical results.

Keywords: Periodic materials, Pantographic metamaterials, Wave propagation, Complex spectrum, Nonlinear dynamics, Perturbation methods.

1. Introduction

The dispersion properties of periodic media have been widely studied over the past century in a multiplicity of different scientific branches, ranging from acoustics of crystal lattices to optics of dielectric gratings [1–3]. Recently, the research interest towards the propagation of elastic waves through periodic mechanical systems has been renewed by the extraordinary developments in the micro/nano-engineering of architected materials and acoustic metamaterials [4–8]. Indeed, the rapid technological progresses in the fields of high-precision manufacturing and high-fidelity prototyping are paving the way for the next generations of artificial materials, with highly customizable dispersion properties.

Within this challenging scenario, a decisive impulse towards the conception of new periodic materials with unusual or functional dispersion properties is given by the virtuous synergy between the descriptive power of different mechanical formulations – covering the largest variety of discrete models and equivalent continua – and the growing resources of computational optimization [9–17]. Particularly, the high parametric tunability of composite microframes (trusses, grillages, honeycombs) favors the development and optimal design of periodic microstructures working as broadband phononic filters, directional energy propagators, acoustic polarizers and non-reciprocal rectifiers [18–24]. As major consequence, the extreme versatility and mul-

*Corresponding author
Email address:* `v.settimi@staff.univpm.it` (Valeria Settimi)

tifunctionality of mechanical metamaterials have been profitably exploited to achieve innovative and fascinating applications, including impact absorption, negative refraction, sound equalization, wave beaming and focusing, vibration shielding, noise silencing and invisibility cloaking [25–33].

Within this rapidly-evolving context, an emerging research trend is targeted at improving the dynamic response of mechanical metamaterials, by overcoming the traditional physical limits inherent to the microstructural inertia, stiffness and damping. Among the others, inhibiting the propagation of low-frequency waves is a major challenge in the microstructural design of high-performant mechanical metamaterial. Indeed, both natural solids and artificial lattices natively possess a low-pass spectral band associated to shear waves [1]. Based on these motivations, the specific objective of realizing functional metamaterials working as low and ultra-low frequency filters for elastic waves has inspired the conception of different original solutions for reducing the centerfrequency of the lowest spectral stop band. Among the others, the mechanical solutions governing the low-frequency response are mostly based on microstructural mechanisms operating at the cell scale, like local resonances, inertia amplification, multi-stability, and trampoline stiffness [34–38].

Inertial amplification can be realized by virtue of an intracellular (local) pantographic mechanism based on rhombic modules of rigid trusses connecting eccentric masses [39–41]. This microstructural scheme grants the inertia-amplifying mechanism a threefold advantage. Firstly, the rigidly-connected eccentric masses do not introduce additional active degrees-of-freedom and – consequently – do not enlarge the dimension of the periodic cell model. Secondly, the pantographic mechanism, being kinematically indeterminate, does not increase the microstructural stiffness and, therefore, does not alter the static performance of the metamaterial. Lastly, the mechanical linkage of hinged rigid bodies required to build up the pantographic scheme is easily realizable from a technological viewpoint [42]. On the other hand, the axial indeformability of the trusses composing the pantograph arms introduces local quadratic and cubic nonlinearities of geometric inertial nature in the finite amplitude regime of oscillations. Although inertial nonlinearities have rarely been analyzed in the framework of infinite periodic media, it is well known that weak nonlinearities may induce significant phenomena in free wave propagation, like amplitude-dependent dispersion properties, superharmonic internal resonances, dynamic bifurcations, solitary waves, non-regular responses, irreversible energy transfers [43–46]. In a general perspective targeted at enhanced functionalization, nonlinearities induce dependence of the spectral properties on the dynamic response amplitude, thus widening – in principle – the space of the tunable functional variables in design and optimization problems.

The free propagation of harmonic waves in weakly nonlinear periodic systems can be studied by employing perturbation methods, which allow to determine the dispersion properties as analytical – although asymptotically approximate – functions of the oscillation amplitudes and the governing parameters. According to this methodological approach, monocoupled and multicoupled periodic system with complement or essential nonlinearities have been studied, both in the absence and in the presence of damping and internal resonances [47–51]. Attention has been primarily focused on symmetric systems characterized by cubic nonlinearities, whereas minor interest has been captured by systems with quadratic nonlinearities [52, 53]. Even lower attention has been devoted to systems featured by coexistent and competing quadratic and cubic nonlinearities. Moreover, although several studies have analyzed one or the other aspect individually, the comprehensive analysis of the simultaneous effects of quadratic and cubic nonlinearities of inertial nature on all the dispersion properties (wavefrequencies *and* waveforms) is an open and rarely explored field of investigation.

Alternatively, the free wave propagation in strongly nonlinear periodic systems can be tackled through analytical and computational techniques, including the map approach and the homotopy method, among the others. In this respect, linearized and nonlinear maps have been used to assess the wave propagation properties of one-dimensional chains of mono- and bi-coupled nonlinear oscillators [54–56]. According to this approach, the mathematical conditions and methodological tools for studying the wave propagation are formally analogous to those employed to assess the linear stability of periodic orbits in dynamic systems. Furthermore, quasi-periodic and chaotic solutions have been also recognized to occur. The homotopy method has been employed to investigate the dynamic response of one-dimensional strongly nonlinear acoustic metamaterials [57, 58]. According to this semi-analytical approach, the geometric concept of homotopy from the mathematical field of topology is employed to generate a convergent series solution. By virtue of this method, the local period-doubling bifurcation of multiple cells has been demonstrated to induce chaotic bands.

Based on this scientific background, the present paper introduces a one-dimensional infinite lattice, char-
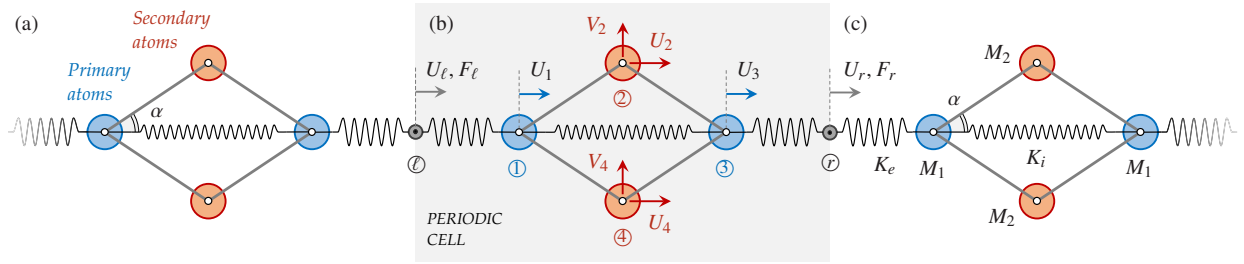
Figure 1: Periodic pantographic material: (a) tetra-atomic unit, (b) periodic cell of the discrete model, (c) mechanical properties.

acterized by a tetra-atomic periodic cell, to realize an original minimal prototype of pantographic metamaterial with inertia amplification (Section 2). According to a classic beam lattice formulation, a kinematically nonlinear discrete model is derived from the Hamilton's principle to describe the free undamped dynamics of the cellular microstructure. The axial indeformability constraint of the pantograph arms determines quadratic and cubic couplings among the active degrees of freedom (Subsection 2.1). Therefore, a general asymptotic strategy based on the Multiple Scale Method is employed to attack the weakly nonlinear governing equations (Section 3). Solving the eigenproblem governing the lowest asymptotic order, the linear dispersion properties are investigated through an invariant representation of the complex-valued frequency band structure (Subsection 3.1). Subsequently, solving the non-homogeneous hierarchical problems at the higher orders, the nonlinear frequencies and waveforms are both determined in closed form as parametric functions of the oscillation amplitude (Subsections 3.2 and 3.3). The accuracy of the analytical solutions is successfully verified by comparing the invariant manifolds associated to the nonlinear waveforms with periodic orbits obtained via numerical integrations of the governing equations (Section 4). Finally, concluding remarks are pointed out.

2. Pantographic material

The minimal physical realization of a pantographic metamaterial with inertial amplification can be represented by a one-dimensional crystal lattice, characterized by a repetitive tetra-atomic unit (Figure 1a). The crystalline microstructure can be synthesized by creating an infinite chain of identical massive disks (*primary atoms*), enriched by lateral massive disks (*secondary atoms*) located symmetrically with respect to the chain axis. The secondary atoms are paired in correspondence of the mid-distance between alternate couples of primary atoms. Consequently, the four (two

primary and two secondary) atoms of the metamaterial unit are organized according to a rhombic geometry in the plane containing all the disk centroid (*metamaterial plane*). The rhombic shape is fully characterized by the distance L separating the primary atoms and the acute angle α between the chain axis and the primary-to-secondary atom alignments (*amplification angle*). Each primary atom is postulated to exchange only conservative position-dependent forces (attraction or repulsion) with the nearest-neighbor elements of the chain. Within a single unit, primary and secondary atoms are supposed to not change their mutual distance.

2.1. Discrete model

From the mechanical viewpoint, the free dynamics of the pantographic metamaterial can properly be described by a low-dimensional discrete model. The periodic cell can be properly selected to coincide with the tetra-atomic unit (Figure 1b). All atoms can be modeled as point masses located at the disk centroids. Consequently, the undeformed configuration of the cellular rhombic microstructure is described by a set of four configurational nodes, located at the rhombus vertices. The respective masses of the primary and secondary atoms M_1 and M_2 are supposed to differ from each other, in the general case (Figure 1c). As key hypothesis, the primary atoms are assumed to possess a single degree-of-freedom, corresponding to the translation along the chain axis. Differently, each secondary atom is supposed to develop a two degrees-of-freedom translation in the metamaterial plane. The unique degree-of-freedom of the two principal atoms can be described by the displacements U_1 and U_3 of the configurational nodes ① and ③. Similarly, the two degrees-of-freedom of the secondary atoms can be described by the displacement components U_2, U_4 and V_2, V_4 (respectively parallel and orthogonal to the chain axis) of the configurational nodes ② and ④. Auxiliary massless nodes ⓛ and ⓡ, characterized by a unique chain-aligned translational degree-of-freedom described by the displace-

3

ments U_ℓ and U_r, are purposely introduced at the left and right sides of the cell boundary, respectively.

The inter-cellular and intra-cellular interactions between the principal atoms are simulated by linear elastic springs. Specifically, two elastic linear springs with stiffness K_e (*external springs*) connect each of the principal atoms with the nearest auxiliary atom at the cell boundary to simulate the inter-cellular interactions. An additional linear spring with stiffness K_i (*internal spring*) connects the two principal atoms to simulate the intra-cellular interactions. The constraint of unchangeable mutual distance between each pair of primary and secondary atoms is introduced by a rigid truss link connecting the respective configurational nodes.

In order to formulate the ordinary-differential equations of motion governing the discrete model in a suited nondimensional form, the following dimensionless displacement variables can be defined

$$u_1 = \frac{U_1}{L}, \quad u_2 = \frac{U_2}{L}, \quad u_3 = \frac{U_3}{L}, \quad u_4 = \frac{U_4}{L} \quad (1)$$
$$v_2 = \frac{V_2}{L}, \quad v_4 = \frac{V_4}{L}, \quad u_\ell = \frac{U_\ell}{L}, \quad u_r = \frac{U_r}{L}$$

and the dimensionless time $\tau = \Omega t$ can be defined by using the (square) frequency $\Omega^2 = K_e/M_1$ as proper reference. The positions $w = u_3 - u_1$ and $u = u_1$ are introduced for the sake of convenience.

As major remark, all the displacements of the massive primary and secondary atoms describe *active* degrees-of-freedom, since inertia forces can actually develop in the nodes at the atom centroids (*internal nodes*). On the contrary, the two displacements of the auxiliary massless nodes at the cell boundaries (*external nodes*) describe *passive* degrees-of-freedom, not associated to the development of inertia forces. Indeed, only quasi-static boundary forces, exerted by the adjacent cells (*inter-cellular forces*), can be applied at the external nodes.

A minimal set $\boldsymbol{\mu}$ of three independent dimensionless parameters, sufficient to describe the mechanical model, is composed by the quantities

$$\varrho^2 = \frac{M_2}{M_1}, \qquad \eta = \frac{K_i}{K_e} \qquad (2)$$

together with the amplification angle $\alpha \in (0, \pi/2)$. From the physical viewpoint, the parameter ϱ^2 describes the secondary-to-primary *mass ratio*, whereas the parameter η represents the internal-to-external *stiffness ratio*. Naturally, the mass and stiffness ratios must be assumed strictly positive ($\varrho^2 > 0$, $\eta > 0$).

The double-symmetry properties that can be recognized with respect to the periodic cell center require that

the secondary atom displacements obey to the relations

$$u_2 = u_4 = u + \tfrac{1}{2}w, \qquad v_2 = -v_4 \qquad (3)$$

where it is worth noting the dependence of the chain-parallel displacements u_2 and u_4 of the secondary atoms on the displacement u and w of the primary atoms.

Furthermore, the indeformability conditions of the rigid truss links connecting the primary and secondary atoms impose the additional asymptotic relation

$$v_4 = p_1 w + p_2 w^2 + 4 p_2 p_1^2 w^3 + O(w^4) \qquad (4)$$

where the α-dependent auxiliary coefficients read

$$p_1 = \tfrac{1}{2} \cot \alpha, \qquad p_2 = \frac{\cot \alpha}{4 \sin^2 \alpha} \qquad (5)$$

and the dependence of the chain-parallel displacements v_4 (and v_2) of the secondary atoms on the *relative displacement w* of the primary atoms can be noted.

2.2. Nonlinear equations of motion

Adopting the undeformed configuration as initial reference for the dynamic equilibrium and considering the symmetry and indeformability conditions (3) and (4), the Hamilton's principle can be applied (see Appendix A). Therefore, the nonlinear equations of motion governing the free dynamics of the periodic cell read

$$2(1+\varrho^2)\ddot{u} + (1+\varrho^2)\ddot{w} + 2u + w - u_\ell - u_r = 0 \quad (6)$$
$$(1+\varrho^2)\ddot{u} + (1+\varrho_e^2)\ddot{w} + u + (1+\eta)w - u_r +$$
$$+ c_2(\dot{w}^2 + 2w\ddot{w}) + c_3 w(\dot{w}^2 + w\ddot{w}) = 0$$

where terms higher than third order in the configuration variables have been neglected. The ϱ^2-dependent amplified inertias are clearly recognizable in the coefficients multiplying all the acceleration terms. In particular, the linear inertia term in the second equation can be further increased by regulating the amplification angle, since the α-dependent auxiliary parameter

$$\varrho_e^2 = \left(\tfrac{1}{2} + 2p_1^2\right)\varrho^2 \qquad (7)$$

obeys to the rule $\varrho_e^2 > \varrho^2$ for the admissible α-values.

The nonlinear dynamic system (6) consists of two homogeneous ordinary differential equations, linearly coupled to each other, governing the free (unconstrained) active degrees of freedom u and w, playing the role of *Lagrangian coordinates*. The second equation is featured by *weak* inertial nonlinearities in the relative displacement w. The nonlinearities are of quadratic and cubic nature, respectively governed by the coefficients

$$c_2 = 4p_1 p_2 \varrho^2, \qquad c_3 = 8p_2(p_2 + 6p_1^3)\varrho^2 \qquad (8)$$

4

which depend linearly on the mass ratio ϱ^2 and trigonometrically on the amplification angle α. This peculiar kind of nonlinearities is well-known to rise up in consequence of indeformability conditions [44]. From the mathematical viewpoint, both coefficients c_2 and c_3 can easily be proved to grow monotonically with increasing mass ratios ϱ^2 and decreasing amplification angles α. In order to justify this characteristic mechanical behaviour, it can be pointed out that the quadratic and cubic nonlinearities have geometric origin and are essentially associated to the constrained displacement components v_2 and v_4 of the secondary atoms (see also Appendix A). Therefore, from the physical viewpoint, reducing the amplification angles maximizes the nonlinearities because lower α-values determine geometrically larger v-contributions in the constrained motion of the secondary atoms, for the same w-displacement in the free motion of the primary atoms.

The Hamilton's principle returns also the linear equations governing the quasi-static equilibrium at the external nodes. Denoting by F_ℓ and F_r the inter-cellular external forces applied at the left and right external nodes, respectively, the equations read

$$u_\ell - u = f_\ell, \qquad u_r - u - w = f_r \qquad (9)$$

where the dimensionless quantities $f_\ell = F_\ell/(K_e L)$ and $f_r = F_r/(K_e L)$. It may be worth noting that the same equations can be equivalently expressed in terms of the internal forces $\sigma_\ell = -f_\ell$ and $\sigma_r = f_r$ developed by the external springs undergoing tension (if $\sigma_\ell > 0$ and $\sigma_r > 0$) or compression ($\sigma_\ell < 0$ and $\sigma_r < 0$).

Collecting all *active* displacements in the configurational coordinate vector $\mathbf{u}_a = (u, w)$ and all *passive* displacements in the vector $\mathbf{u}_p = (u_\ell, u_r)$, the equations of motion (6) and the quasi-static equations (9) can conveniently be expressed in the matrix form

$$\mathbf{M}\ddot{\mathbf{u}}_a + \mathbf{K}_{aa}\mathbf{u}_a + \mathbf{K}_{ap}\mathbf{u}_p + \mathbf{n}(\mathbf{u}_a, \dot{\mathbf{u}}_a, \ddot{\mathbf{u}}_a) = \mathbf{0} \qquad (10)$$
$$\mathbf{K}_{pa}\mathbf{u}_a + \mathbf{K}_{pp}\mathbf{u}_p = \mathbf{f}_p$$

where the mass and stiffness matrices are

$$\mathbf{M} = \begin{bmatrix} 2(1+\varrho^2) & 1+\varrho^2 \\ 1+\varrho^2 & 1+\varrho_e^2 \end{bmatrix}, \quad \mathbf{K}_{aa} = \begin{bmatrix} 2 & 1 \\ 1 & 1+\eta \end{bmatrix} \,(11)$$

$$\mathbf{K}_{ap} = \begin{bmatrix} -1 & -1 \\ 0 & -1 \end{bmatrix}, \quad \mathbf{K}_{pp} = \begin{bmatrix} 1 & 0 \\ 0 & 1 \end{bmatrix}$$

while the stiffness matrix $\mathbf{K}_{pa}^\top = \mathbf{K}_{ap}$. The vector of quadratic and cubic nonlinearities is

$$\mathbf{n}(\mathbf{u}_a, \dot{\mathbf{u}}_a, \ddot{\mathbf{u}}_a) = \begin{pmatrix} 0 \\ c_2(\dot{w}^2 + 2w\ddot{w}) + c_3 w(\dot{w}^2 + w\ddot{w}) \end{pmatrix} \,(12)$$

and the vector of passive forces is $\mathbf{f}_p = (f_\ell, f_r)$.

Alternately, introducing the active velocity vector $\mathbf{v}_a = (\dot{u}, \dot{w})$ and joining the active velocity and displacement vectors into the state space vector $\mathbf{z} = (\mathbf{u}_a, \mathbf{v}_a)$, the dynamic system (10) can be expressed as

$$\mathbf{A}\dot{\mathbf{z}} + \mathbf{B}\mathbf{z} + \mathbf{C}\mathbf{u}_p = \mathbf{c}(\mathbf{z}, \dot{\mathbf{z}}) \qquad (13)$$
$$\mathbf{D}\mathbf{z} + \mathbf{K}_{pp}\mathbf{u}_p = \mathbf{f}_p$$

where the governing matrices are

$$\mathbf{A} = \begin{bmatrix} \mathbf{O} & \mathbf{M} \\ \mathbf{M} & \mathbf{O} \end{bmatrix}, \quad \mathbf{B} = \begin{bmatrix} \mathbf{K}_{aa} & \mathbf{O} \\ \mathbf{O} & -\mathbf{M} \end{bmatrix}, \quad \mathbf{C} = \begin{bmatrix} \mathbf{K}_{ap} \\ \mathbf{O} \end{bmatrix} \,(14)$$

while the vector of quadratic and cubic nonlinearities at the right-hand of equation (13) is

$$\mathbf{c}(\mathbf{z}, \dot{\mathbf{z}}) = \begin{pmatrix} -\mathbf{n}(\mathbf{z}, \dot{\mathbf{z}}) \\ \mathbf{0} \end{pmatrix} \qquad (15)$$

and the matrix $\mathbf{D} = \mathbf{C}^\top$. It may be worth remarking that, among the other equivalent expressions of the dynamic system in the state space, the form (13) preserves the symmetry of the square matrices $\mathbf{A}$ and $\mathbf{B}$.

3. Asymptotic approach to wave propagation

Following a general computational strategy formulated for determining the nonlinear frequencies and nonlinear normal modes of structural systems [59], the asymptotic Method of Multiple Scales can be adopted to determine in a suited analytical – although approximate – fashion how the dispersion properties (wavefrequencies and waveforms) nonlinearly depend on the oscillation amplitude of the propagating wave.

According with the classic perturbation scheme for systems with quadratic and cubic nonlinearities [60], a small dimensionless parameter $\epsilon \ll 1$ can be introduced for ordering purposes and the solutions of the nonlinear equation (13) are sought in the approximate form of a power series expansion truncated at the third ϵ-power

$$\mathbf{z} = \epsilon\, \mathbf{z}_1(T_0, T_1, T_2) + \epsilon^2 \mathbf{z}_2(T_0, T_1, T_2) + \qquad (16)$$
$$+ \epsilon^3 \mathbf{z}_3(T_0, T_1, T_2) + O(\epsilon^4)$$
$$\mathbf{u}_p = \epsilon\, \mathbf{u}_{p1}(T_0, T_1, T_2) + \epsilon^2 \mathbf{u}_{p2}(T_0, T_1, T_2) +$$
$$+ \epsilon^3 \mathbf{u}_{p3}(T_0, T_1, T_2) + O(\epsilon^4)$$
$$\mathbf{f}_p = \epsilon\, \mathbf{f}_{p1}(T_0, T_1, T_2) + \epsilon^2 \mathbf{f}_{p2}(T_0, T_1, T_2) +$$
$$+ \epsilon^3 \mathbf{f}_{p3}(T_0, T_1, T_2) + O(\epsilon^4)$$

where $T_0 = \tau$ is the fast time-scale characterizing the harmonic wave motions at the linear frequencies and $T_j = \epsilon^j \tau$ are slow time-scales ($j = 1, 2$). Accordingly,

the ordinary time-derivative $d/d\tau$ is expressed by the partial derivatives $D_j = \partial/\partial T_j$ as $D_0 + \epsilon D_1 + \epsilon^2 D_2 + \dots$.

Introducing the expansion (16) into the nonlinear ordinary differential equation (13) and equating all the terms of like ϵ-powers yields a ordered hierarchy of linear partial differential equation *pairs*

- Order ϵ $\qquad \mathbf{A}D_0\mathbf{z}_1 + \mathbf{B}\mathbf{z}_1 + \mathbf{C}\mathbf{u}_{p1} = \mathbf{0}$ $\qquad$ (17)

$$\mathbf{D}\mathbf{z}_1 + \mathbf{K}_{pp}\mathbf{u}_{p1} = \mathbf{f}_{p1}$$

- Order ϵ^2 $\qquad \mathbf{A}D_0\mathbf{z}_2 + \mathbf{B}\mathbf{z}_2 + \mathbf{C}\mathbf{u}_{p2} = \mathbf{b}_2(\mathbf{z}_1)$

$$\mathbf{D}\mathbf{z}_2 + \mathbf{K}_{pp}\mathbf{u}_{p2} = \mathbf{f}_{p2}$$

- Order ϵ^3 $\qquad \mathbf{A}D_0\mathbf{z}_3 + \mathbf{B}\mathbf{z}_3 + \mathbf{C}\mathbf{u}_{p3} = \mathbf{b}_3(\mathbf{z}_1, \mathbf{z}_2)$

$$\mathbf{D}\mathbf{z}_3 + \mathbf{K}_{pp}\mathbf{u}_{p3} = \mathbf{f}_{p3}$$

where the operators governing the left-hand part of the equation pairs are independent of the order.

The free propagation of elastic waves through the mechanical metamaterial can be analyzed by means of the Floquet-Bloch theory for linear periodic structures [1]. Accordingly, a class of harmonic wave solutions can be obtained by enforcing at each ϵ^n-order ($n = 1, 2, 3$) the *quasi-periodicity* exponential relations

$$u_{rn} = \mathrm{e}^{-\iota\beta}u_{\ell n}, \qquad\qquad f_{rn} = -\mathrm{e}^{-\iota\beta}f_{\ell n} \qquad (18)$$

between the passive variables (two displacements and two forces) at the opposite sides of the periodic cell. Equations (18) can conveniently be expressed in the matrix form $\mathbf{u}_{pn} = \mathbf{L}u_{\ell n}$ and $\mathbf{f}_{pn} = \mathbf{N}f_{\ell n}$, where

$$\mathbf{L} = \begin{bmatrix} 1 \\ \mathrm{e}^{-\iota\beta} \end{bmatrix}, \qquad \mathbf{N} = \begin{bmatrix} 1 \\ -\mathrm{e}^{-\iota\beta} \end{bmatrix} \qquad (19)$$

and β is the nondimensional wavenumber, spanning the one-dimensional Brillouin zone $\mathcal{B} = [-\pi, \pi]$.

Imposing the quasi-periodicity relations (18) allows the systematic reduction of the system dimension at each ϵ^n-order, by quasi-statically condensing the passive displacements $\mathbf{u}_{pn}$. Consequently, the hierarchy of equation *pairs* (17) can be condensed in the reduced space of the active state space variables $\mathbf{z}_n$. Therefore, after condensation, the free propagation of weakly nonlinear waves through the pantographic metamaterial is governed by the ordered hierarchy of linear partial differential *perturbation equations*

- Order ϵ $\qquad \mathbf{A}D_0\mathbf{z}_1 + \tilde{\mathbf{B}}\mathbf{z}_1 = \mathbf{0}$ $\qquad$ (20)

- Order ϵ^2 $\qquad \mathbf{A}D_0\mathbf{z}_2 + \tilde{\mathbf{B}}\mathbf{z}_2 = \mathbf{b}_2(\mathbf{z}_1)$

- Order ϵ^3 $\qquad \mathbf{A}D_0\mathbf{z}_3 + \tilde{\mathbf{B}}\mathbf{z}_3 = \mathbf{b}_3(\mathbf{z}_1, \mathbf{z}_2)$

where the β-dependent matrix $\tilde{\mathbf{B}}$ can be expressed as

$$\tilde{\mathbf{B}} = \mathbf{B} - \mathbf{C}\mathbf{L}(\mathbf{L}^\dagger\mathbf{K}_{pp}\mathbf{L})^{-1}\mathbf{L}^\dagger\mathbf{D} \qquad (21)$$

and $()^\dagger$ indicates the conjugate transpose. The matrix $\tilde{\mathbf{B}}$ is Hermitian (that is $\tilde{\mathbf{B}}^\dagger = \tilde{\mathbf{B}}$) by construction, and becomes singular at the limit of *long wavelengths* ($\beta = 0$).

From the mathematical viewpoint, the lowest order of the ordered hierarchy of differential equations (20) establishes a homogeneous (free vibration) problem in the unknown variable $\mathbf{z}_1$. Once all the lowest order solutions (*generating solutions*) are known, the n-th higher order establishes a non-homogeneous (forced vibration) problem in the unknown variable $\mathbf{z}_n$, with forcing term depending on all the lower-order solutions. For the sake of completeness, the condensed passive displacements $\mathbf{u}_{pn}$ and forces $\mathbf{f}_{pn}$ can be determined a posteriori at each order, if necessary. Indeed, they quasi-statically depend on the active variables $\mathbf{z}_n$ through the relations

$$\mathbf{u}_{pn} = -\mathbf{L}(\mathbf{L}^\dagger\mathbf{K}_{pp}\mathbf{L})^{-1}\mathbf{L}^\dagger\mathbf{D}\,\mathbf{z}_n \qquad (22)$$

$$\mathbf{f}_{pn} = \left(\mathbf{I} - \mathbf{K}_{pp}\mathbf{L}(\mathbf{L}^\dagger\mathbf{K}_{pp}\mathbf{L})^{-1}\mathbf{L}^\dagger\right)\mathbf{D}\,\mathbf{z}_n$$

where it can be recalled that the rectangular stiffness matrix $\mathbf{D} = [\mathbf{K}_{pa}, \mathbf{O}]$, to clarify that the passive variables do not depend on the active velocities in the $\mathbf{z}_n$-vector.

From the methodological viewpoint, it must be remarked that the condensation procedure (including the imposition of the quasi-periodicity relations) is essentially founded on the linearity of the quasi-static relation $\mathbf{D}\mathbf{z}_n + \mathbf{K}_{pp}\mathbf{u}_{pn} = \mathbf{f}_{pn}$ between the passive and active variables at each order. In a broader perspective, all the algebraic manipulations of the governing matrices are possible by virtue of the linearity of the intercellular coupling, independently of the coupling dimension. Specifically, mono-coupled [47] as well as multicoupled periodic systems [56] characterized by local (namely intracellular or *on-site*) nonlinearities could be treated within the same analytical framework. The condensation scheme is also formally valid and straightforwardly extendible to bi-dimensional and three-dimensional periodic systems, with proper adjustments. Consequently, the methodological strategy can be considered quite general, and applicable to a class of mechanical metamaterials featured by similar periodic microstructures.

3.1. Linear dispersion properties

The linear homogeneous problem governing the lowest order of perturbation equations (20) can be tackled by imposing the harmonic solution $\mathbf{z}_1 = \mathbf{y}\exp(\lambda T_0)$. Eliminating the dependence on the fast time T_0 gives the linear eigenproblem

$$\left(\tilde{\mathbf{B}} + \lambda\mathbf{A}\right)\mathbf{y} = \mathbf{0} \qquad (23)$$

whose solution returns four eigenpairs $(\lambda, \mathbf{y})$, composed by the eigenvalues λ_i and the corresponding eigenvectors $\mathbf{y}_i$, spanning the complete eigenspace of the state variables ($i = 1, ..., 4$). By virtue of the $\tilde{\mathbf{B}}$-matrix properties, the eigenproblem (23) is actually satisfied by two purely imaginary eigenvalues λ_1 e λ_2 and their complex conjugates $\lambda_3 = \bar{\lambda}_1$ and $\lambda_4 = \bar{\lambda}_2$ (where the bar indicates complex conjugate), which can be ordered in the diagonal matrix $\mathbf{\Lambda} = \mathrm{diag}(\lambda_1, \lambda_2, \lambda_3, \lambda_4)$. The corresponding eigenvectors are complex-valued in the general case and can be ordered columnwise in the matrix $\mathbf{Y} = [\mathbf{y}_1, \mathbf{y}_2, \mathbf{y}_3, \mathbf{y}_4]$. The eigenvalue and eigenvector matrices can suitably be expressed in the partitioned form

$$\mathbf{\Lambda} = \begin{bmatrix} \iota\mathbf{\Omega} & \mathbf{O} \\ \mathbf{O} & -\iota\mathbf{\Omega} \end{bmatrix}, \qquad \mathbf{Y} = \begin{bmatrix} \mathbf{\Phi} & \mathbf{\Phi} \\ -\iota\mathbf{\Omega}\mathbf{\Phi} & \iota\mathbf{\Omega}\mathbf{\Phi} \end{bmatrix} \qquad (24)$$

where $\mathbf{\Omega} = \mathrm{diag}(\omega^-, \omega^+)$ is the diagonal matrix collecting the two β-dependent wavefrequencies

$$\omega^\mp = \left[\tfrac{1}{2}\mathcal{J}_1(\beta) \mp \left(\mathcal{J}_1(\beta)^2 - 4\mathcal{J}_2(\beta) \right)^{1/2} \right]^{1/2} \qquad (25)$$

while $\mathbf{\Phi} = [\boldsymbol{\phi}^-, \boldsymbol{\phi}^+]$ is a two-by-two matrix. It collects columnwise the two β-dependent waveforms (normalized with respect to the active u-coordinate)

$$\boldsymbol{\phi}^\mp = \left(1, \frac{\cos\beta - 1 + 2(\omega^\mp)^2(1 + \varrho^2) - \iota\sin\beta}{1 + 2\eta - 2(\omega^\mp)^2(1 + \varrho_e^2)} \right) \qquad (26)$$

that can be easily verified to become real-valued vectors at the limits of long wavelengths ($\beta = 0$) and short wavelengths ($\beta = \pm\pi$). The two β-dependent auxiliary variables that have been introduced in equation (25) read

$$\mathcal{J}_1(\beta) = \frac{1 + \varrho_e^2 + 2\eta(1 + \varrho^2) + (\varrho^2 - \varrho_e^2)\cos\beta}{1 - \varrho^4 + 2(1 + \varrho^2)\varrho_e^2} \qquad (27)$$

$$\mathcal{J}_2(\beta) = \frac{\eta(1 - \cos\beta)}{1 - \varrho^4 + 2(1 + \varrho^2)\varrho_e^2}$$

and could be employed to reduce the linear dispersion properties to a proper invariant representation for mono-, bi- and three-coupled periodic systems [61, 62].

Within the limit of small (ϵ-order) oscillation amplitudes, the wavefrequencies (25) and waveforms (26) characterize the unitary-amplitude harmonic waves of the form $\mathbf{u}_a = \boldsymbol{\phi}^\mp \exp(\iota\omega^\mp T_0 - \iota\beta)$ that freely propagate with a certain wavenumber β through the pantographic metamaterial characterized by the mechanical parameters $(\varrho^2, \eta, \alpha)$. Therefore, the wavefrequencies $\omega^\mp$ and the waveforms $\boldsymbol{\phi}^\mp$ will be referred to as the linear dispersion properties in the following. Without loss of generality, focus can be put on the *forward* propagating waves, described by positive wavefrequencies ($\omega^\mp \geq 0$)

depending on positive wavenumbers β ranging in the $\mathcal{B}$-subdomain $\mathcal{B}_1 = [0, \pi]$. According to the assumptions made for the physical parameters, the discriminant quantity $\mathcal{J}_1(\beta)^2 - 4\mathcal{J}_2(\beta)$ is positive. Consequently, the inequality $\omega^- \leq \omega^+$ holds in the entire $\mathcal{B}_1$-domain. Therefore, from the physical viewpoint, the dispersion functions $\omega^-(\beta)$ and $\omega^+(\beta)$ describe the lower-frequency curve (*acoustic branch*) and the higher-frequency curve (*optical branch*) characterizing the dispersion spectrum of the pantographic metamaterial, respectively. By extension, ω^- and ω^+ can also be referred to as the (linear) acoustic and optical frequencies, respectively. Similarly, $\boldsymbol{\phi}^-$ and $\boldsymbol{\phi}^+$ can be referred to as the (linear) acoustic and optical waveforms.

The band structure of the linear dispersion spectrum can be discussed by analytically distinguishing the *pass bands* from the *stop bands*, corresponding to the distinct frequency ranges in which the harmonic waves can propagate without attenuation or cannot propagate due to an exponential spatial decay, respectively. To this purpose, it may be convenient to invert the relation $\omega(\beta)$, by considering the wavefrequency ω as independent real parameter and the wavenumber $\beta(\omega)$ as eigenproblem unknown in the complex plane. The essential advantage is that the wave propagation problem can straightforwardly be realigned with the well-established methodological framework of the transfer matrix techniques, widely employed to analyze the dispersion properties of periodic structures with low-dimension intercellular couplings [61, 63–65]. Indeed, the β-dependent matrix $\tilde{\mathbf{B}}$ can be reformulated in the form

$$\tilde{\mathbf{B}} = \mathbf{R}_0 + \mathbf{R}_1\,\mathrm{e}^{\iota\beta} + \mathbf{R}_2\,\mathrm{e}^{-\iota\beta} \qquad (28)$$

according to a mathematical procedure generally valid for one-dimensional periodic systems [66] (but also extendible to bi-dimensional periodic systems). Consequently, eigenproblem (23) becomes

$$\left(\tilde{\mathbf{R}}_0(\omega) + \mathbf{R}_1\,\mathrm{e}^{\iota\beta} + \mathbf{R}_2\,\mathrm{e}^{-\iota\beta} \right)\mathbf{y} = \mathbf{0} \qquad (29)$$

with the ω-dependent matrix $\tilde{\mathbf{R}}_0(\omega) = \mathbf{R}_0 + \omega^2\mathbf{A}$. By letting $\mu = \mathrm{e}^{\iota\beta}$ and multiplying by $\mathrm{e}^{\iota\beta}$, equation (29) can be reformulated as

$$\left(\mathbf{R}_1\mu^2 + \tilde{\mathbf{R}}_0(\omega)\mu + \mathbf{R}_2 \right)\mathbf{y} = \mathbf{0} \qquad (30)$$

where the matrices $\mathbf{R}_1$ and $\mathbf{R}_2$ can be proved to be singular. For the pantographic metamaterial, the auxiliary matrices $\mathbf{R}_0, \mathbf{R}_1, \mathbf{R}_2$ are detailed in Appendix B.1. The eigensolution is given by the two roots of the quadratic characteristic polynomial

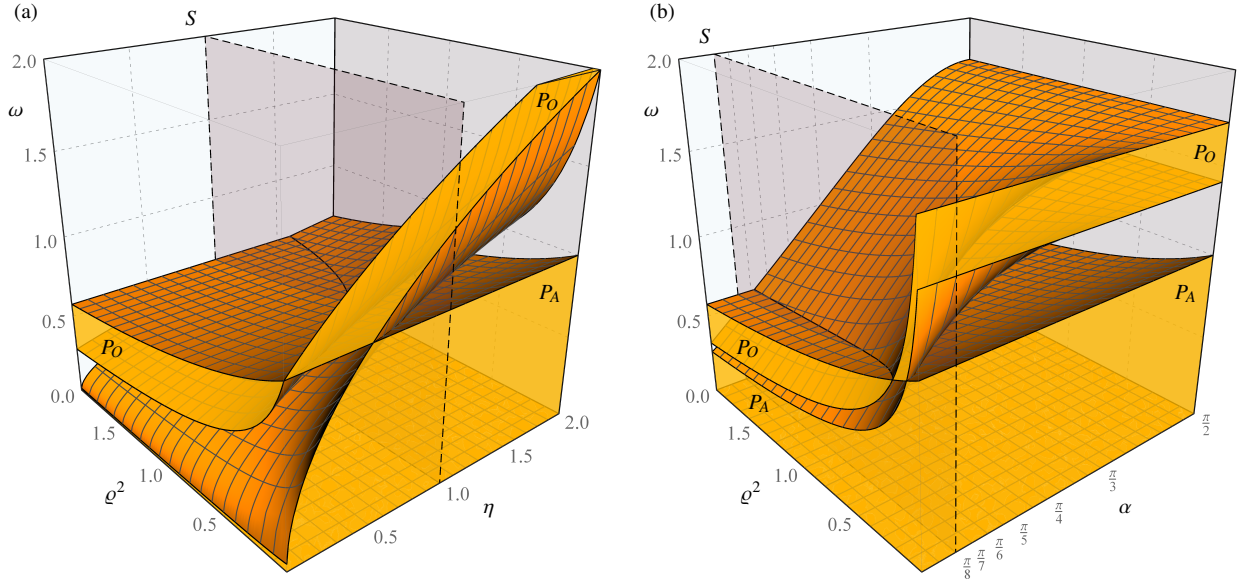$$P(\mu) = \mu^2 + \mathcal{J}(\omega)\mu + 1 \qquad (31)$$

Figure 2: Pass and stop regions of the pantographic metamaterial over (a) the parameter space (ϱ^2, η) for the amplification angle $\alpha = \pi/8$, (b) the parameter space (ϱ^2, α) for the stiffness ratio $\eta = 1$.

where the governing coefficient $\mathcal{J}(\omega)$ is real-valued for undamped systems. Since the polynomial is palindromic, its roots are μ_1 and $\mu_2 = 1/\mu_1$. Depending on the coefficient $\mathcal{J}(\omega)$, three fundamental cases can occur

i) μ_1, μ_2 complex conjugates if $-2 < \mathcal{J}(\omega) < 2$.

ii) μ_1, μ_2 real and distinct if $\mathcal{J}(\omega) < -2 \cup \mathcal{J}(\omega) > 2$

iii) μ_1, μ_2 real and coincident if $\mathcal{J}(\omega) = \pm 2$

Invoking the formal analogy with the Floquet theory for the stability of dynamical systems [54, 61, 67], the three cases correspond to (i) complex-valued roots μ_1, μ_2 sitting on the unitary circle of the complex plane, identifying pass bands in the frequency axis (the analogous of stable regions corresponding to elliptic fixed points), (ii) real-valued roots μ_1, μ_2 lying inside and outside the unitary circle of the complex plane, respectively, and identifying stop bands in the frequency axis (the analogous of unstable regions corresponding to hyperbolic or reflective hyperbolic fixed points), (iii) real valued and coincident roots μ_1, μ_2 sitting on the unitary circle of the complex plane, identifying boundaries between pass and stop bands (the analogous of bifurcation loci corresponding to parabolic fixed points). It may be worth noting that, in the absence of damping, the roots μ_1, μ_2 of the fundamental case (i) are purely imaginary.

Once the roots μ_1, μ_2 of the characteristic polynomial are known, the complex-valued wavenumber β can be

determined by inverting the relation $\mu = e^{\iota\beta}$, yielding

$$\beta = \arg\left(\mu(\omega)\right) - \tfrac{1}{2}\iota \log\left(|\mu(\omega)|^2\right) \qquad (32)$$

which, for the fundamental cases, returns (i) real-valued wavenumbers $\beta \in \mathcal{B}$ of the *dispersion curves* falling within the pass bands, (ii) imaginary-valued wavenumbers β of the *attenuation curves* falling within the stop bands, where the opposite of the imaginary part stands for the attenuation factor of the decaying wave, (iii) real-valued wavenumbers $\beta = n\pi$ (with $n \in \mathbb{Z}$).

For the metamaterial under investigation, the coefficient governing the palindromic polynomial (31) is

$$\mathcal{J}(\omega) = \frac{2\left(2\eta - \varrho^2\omega^2 \csc^2\alpha\right)\left(r_1\omega^2 - 1\right) + 4\omega^2\left(r_2\omega^2 + 1\right)}{2\eta + \varrho^2\omega^2(1 - \cot^2\alpha)} \qquad (33)$$

where $r_1 = 2(\varrho^2 + 1)$ and $r_2 = \varrho^4 - 1$. The transition between the pass and stop regions in the frequency-parameter space is associated to the $(\omega, \alpha, \eta, \varrho^2)$-loci satisfying the condition (iii), requiring $\mathcal{J}(\omega) = \pm 2$. For the pantographic metamaterial, the subcondition $\mathcal{J}(\omega) = 2$ defines the locus $\mathcal{T}_{ps}^r = \bigcup\{\omega_1^2, \omega_2^2\}$, while the subcondition $\mathcal{J}(\omega) = -2$ defines the locus $\mathcal{T}_{ps} = \bigcup\{\omega_3^2, 0\}$, where
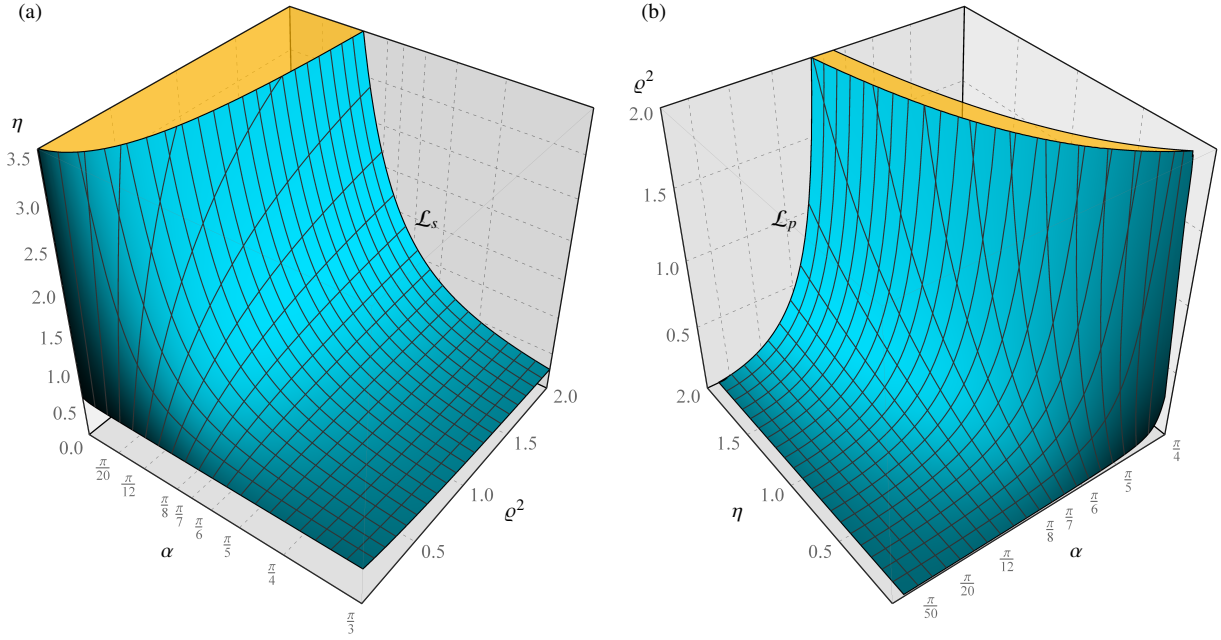
Figure 3: Loci in the mechanical parameter space $(\alpha, \eta, \varrho^2)$: (a) locus $\mathcal{L}_s$ corresponding to vanishing of the stop band, (b) locus $\mathcal{L}_p$ corresponding to vanishing of the optical pass band.

the ω^2-functions are analytically determined as

$$\omega_1^2 = \frac{1}{1+\varrho^2}, \tag{34}$$

$$\omega_2^2 = \frac{4\eta \sin^2 \alpha}{1+\varrho^2 + \cos(2\alpha)(\varrho^2 - 1)},$$

$$\omega_3^2 = \frac{1+2\eta}{1+\varrho^2 \cot^2 \alpha}$$

Moreover, the locus $\mathcal{T}_{ss}$ corresponding to the vanishing of the $\mathcal{J}(\omega)$-denominator is associated to the boundary separating two stop subregions (from hyperbolic to reflective hyperbolic fixed points or viceversa in the analogy with the Floquet theory).

Figure 2 illustrates the pass bands (yellow regions with acoustic band P_A and optical band P_O) and stop bands (white regions) of the pantographic metamaterial over a significant portion of the parametric spaces spanned by the (ϱ^2, η)-pair (Figure 2a) and the (ϱ^2, α)-pair (Figure 2b). The band structure is characterized by two fully separated pass bands. The low-frequency pass band is associated to the acoustic branch, while the high-frequency pass band is associated to the optical branch of the spectrum. The pass bands are separated by a stop band (band gap), whose amplitude normalized with respect to its centerfrequency (relative band gap

amplitude) can be determined analytically as

$$\Delta = \frac{|\min(\omega_1, \omega_3) - \omega_2|}{\min(\omega_1, \omega_2) + \frac{1}{2}|\min(\omega_1, \omega_3) - \omega_2|}. \tag{35}$$

The relative band gap amplitude Δ is mainly dependent on the mass ratio ϱ^2 and the stiffness ratio η. In particular, both the band gap amplitude at the numerator and the centerfrequency at the denominator decrease for increasing ϱ^2-values. For sufficiently large η-values, both the band gap amplitude and the centerfrequency increase for growing η-values.

The band structure shows the existence of parameter combinations corresponding to the vanishing of either the stop band or the optical pass band. These particular conditions are associated to the relations $\omega_1^2 = \omega_2^2$ (vanishing stop band) and $\omega_1^2 = \omega_3^2$ (vanishing optical pass band). The corresponding loci $\mathcal{L}_s$ and $\mathcal{L}_p$ in the parameter space are defined analytically as

$$\mathcal{L}_s: \quad \eta - \frac{1+\varrho^2 \cot^2 \alpha}{2(1+\varrho^2)} = 0, \tag{36}$$

$$\mathcal{L}_p: \quad \eta + \frac{\varrho^2(1-\cot^2 \alpha)}{2(1+\varrho^2)} = 0$$

and are illustrated in Figure 3. Focusing first on the locus $\mathcal{L}_s$, for a fixed mass ratio ϱ^2, the stiffness ratio η significantly grows up for decreasing inertia amplification
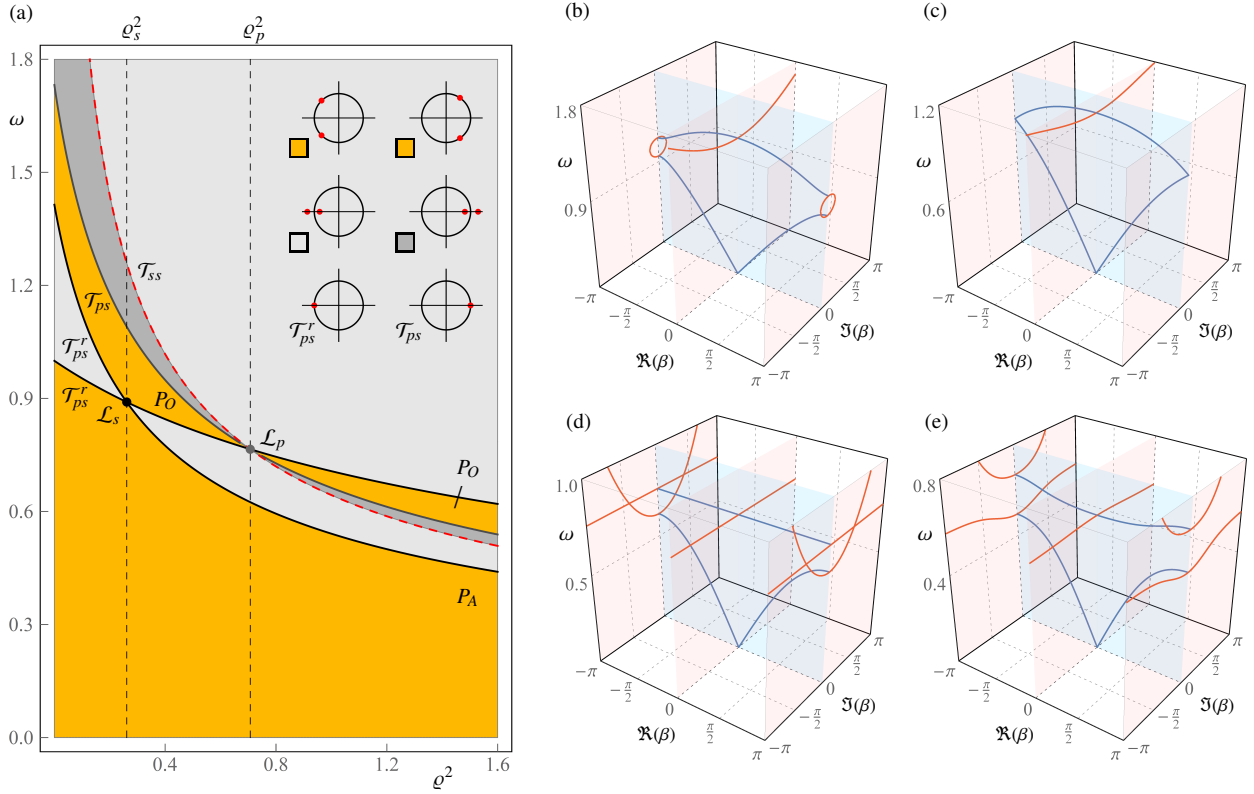
9

Figure 4: Frequency band structure of the pantographic metamaterial (a) pass band (acoustic P_A and optical P_O) and stop band versus the mass ratio ϱ^2 for amplification angle $\alpha = \pi/8$ and stiffness ratio $\eta = 1$, (b)-(e) complex-valued spectra with dispersion curves (blue branches lying in the light blue plane) and attenuation curves (red branches lying in the light red planes) for the mass ratios $\varrho_1^2 = 9/100, \varrho_s^2, \varrho_p^2, \varrho_2^2 = 121/100$.

angles α. Differently, for large α-values, the stiffness ratio η is less sensitive to variations of the mass ratio ϱ^2. Then, considering the locus $\mathcal{L}_p$, for a fixed stiffness ratio η, the mass ratio ϱ^2 significantly increases for growing α-angles. Differently, for small α-values, the mass ratio ϱ^2 is less sensitive to variations of the stiffness ratio η. From equations (36) it is straightforward to demonstrate that – for fixed ϱ^2 – the locus $\mathcal{L}_p$ occurs at lower η-values (for fixed α) or at lower α-values (for fixed η) with respect to the locus $\mathcal{L}_s$.

The planar section S of the band structure reported in Figure 2 for fixed parameters $\alpha = \pi/8, \eta = 1$ is illustrated in Figure 4a. The pass bands (yellow regions with acoustic band P_A and optical band P_O) and stop bands (gray subregions) are plotted versus the varying parameter ϱ^2, together with the transition curves corresponding to the loci $\mathcal{T}_{ps}^r$ (black lines) and $\mathcal{T}_{ps}$ (gray line). The curve corresponding to the locus $\mathcal{T}_{ss}$ is also identified (dashed red line) and the points belonging to the loci $\mathcal{L}_s$ (black dot) and $\mathcal{L}_p$ (gray dot) are marked. For each region and pass-to-stop transition curve, the

position of the Floquet multipliers μ_1, μ_2 with respect to the unitary circle in the complex plane is schematized. A selection of complex-valued spectra illustrating the frequency ω versus the real and imaginary parts of the wavenumber β for significant ϱ^2-values is also reported (Figure 4b-e). The spectra are featured by dispersion curves in the $(\omega, \Re(\beta))$-plane (blue lines), covering the frequency range of the pass bands, and attenuation curves in the $(\omega, \Im(\beta))$-plane (red lines), covering the frequency range of the stop bands. The vanishing of the band gap can be observed for the significant mass ratio $\varrho_s^2 \in \mathcal{L}_s$ in Figure 4c, caused by the crossing between the acoustic and optical curves at the limit of short wavelength ($\beta = \pi$). Furthermore, the vanishing of the optical pass band can be observed for the significant mass ratio $\varrho_p^2 \in \mathcal{L}_p$ in Figure 4d, caused by the β-independence of the optical curve. It is worth noting that a qualitative change in the behaviour of the attenuation curves occurs when moving from low to high values of the mass ratio ϱ^2 (compare Figures 4b and 4e).

10

3.2. Wave propagation in nonlinear regime

Since the left-hand governing matrices $\mathbf{A}$ and $\tilde{\mathbf{B}}$ in the cascade of equations (20) are independent of the order, the linear waveforms obtained from the first-order equation represent a suited base to apply a systematic change of coordinates at each order. Specifically, if the matrix $\mathbf{\Phi}$ is conveniently built by employing properly orthonormalized waveforms $\boldsymbol{\varphi}^{\mp} = n^{\mp}\boldsymbol{\phi}^{\mp}$, the mass-orthogonality relation $\mathbf{\Phi}^{\dagger}\mathbf{M}\mathbf{\Phi} = \mathbf{I}$ holds. The two orthonormalization factors $n^{\mp}$ are reported in Appendix B.2. Therefore, moving to the orthonormal coordinates $\mathbf{q}_k = (q_k^-, q_k^+)$ and $\mathbf{p}_k = (p_k^-, p_k^+)$ through the relation

$$\mathbf{z}_k = \begin{pmatrix} \mathbf{u}_{ak} \\ \mathbf{v}_{ak} \end{pmatrix} = \begin{bmatrix} \mathbf{\Phi} & \mathbf{O} \\ \mathbf{O} & \mathbf{\Phi} \end{bmatrix} \begin{pmatrix} \mathbf{q}_k \\ \mathbf{p}_k \end{pmatrix} \qquad (37)$$

the ordered hierarchy of *perturbation equations* reads

- Order ϵ $D_0\mathbf{p}_1 + \mathbf{\Omega}^2\mathbf{q}_1 = \mathbf{0}$ (38)
  $$D_0\mathbf{q}_1 - \mathbf{p}_1 = \mathbf{0}$$
- Order ϵ^2 $D_0\mathbf{p}_2 + \mathbf{\Omega}^2\mathbf{q}_2 = \mathbf{d}_2(\mathbf{q}_1, \mathbf{p}_1)$
  $$D_0\mathbf{q}_2 - \mathbf{p}_2 = \mathbf{g}_2(\mathbf{q}_1, \mathbf{p}_1)$$
- Order ϵ^3 $D_0\mathbf{p}_3 + \mathbf{\Omega}^2\mathbf{q}_3 = \mathbf{d}_3(\mathbf{q}_1, \mathbf{p}_1, \mathbf{q}_2, \mathbf{p}_2)$
  $$D_0\mathbf{q}_3 - \mathbf{p}_3 = \mathbf{g}_3(\mathbf{q}_1, \mathbf{p}_1, \mathbf{q}_2, \mathbf{p}_2)$$

where the operators governing the left-hand part of the equation pairs are still independent of the order. The not-null right-hand terms, which can also be referred to as *defects of homogeneity*, read

$$\mathbf{d}_2 = -D_1\mathbf{p}_1 - d_2(\mathbf{q}_1, \mathbf{p}_1)\,\boldsymbol{\varphi}_w \qquad (39)$$
$$\mathbf{g}_2 = -D_1\mathbf{q}_1$$
$$\mathbf{d}_3 = -D_1\mathbf{p}_2 - D_2\mathbf{p}_1 - d_3(\mathbf{q}_1, \mathbf{p}_1, \mathbf{q}_2, \mathbf{p}_2)\,\boldsymbol{\varphi}_w$$
$$\mathbf{g}_3 = -D_1\mathbf{q}_2 - D_2\mathbf{q}_1.$$

Two scalar quantities have been introduced to account for the nonlinearities at the second order

$$d_2 = c_2(\boldsymbol{\varphi}_w^\top\mathbf{p}_1)^2 + c_2(\boldsymbol{\varphi}_w^\top\mathbf{q}_1)(\boldsymbol{\varphi}_w^\top D_0\mathbf{p}_1) \qquad (40)$$

and at the third order

$$d_3 = 2c_2(\boldsymbol{\varphi}_w^\top\mathbf{p}_1)(\boldsymbol{\varphi}_w^\top\mathbf{p}_2) + 2c_2(\boldsymbol{\varphi}_w^\top\mathbf{q}_1)(\boldsymbol{\varphi}_w^\top D_0\mathbf{p}_2) + \quad (41)$$
$$+ 2c_2(\boldsymbol{\varphi}_w^\top\mathbf{q}_1)(\boldsymbol{\varphi}_w^\top D_1\mathbf{p}_1) + 2c_2(\boldsymbol{\varphi}_w^\top\mathbf{q}_2)(\boldsymbol{\varphi}_w^\top D_0\mathbf{p}_1) +$$
$$+ c_3(\boldsymbol{\varphi}_w^\top\mathbf{q}_1)(\boldsymbol{\varphi}_w^\top\mathbf{p}_1)^2 + c_3(\boldsymbol{\varphi}_w^\top\mathbf{q}_1)(\boldsymbol{\varphi}_w^\top\mathbf{q}_1)(\boldsymbol{\varphi}_w^\top D_0\mathbf{p}_1)$$

where the complex-valued column vector $\boldsymbol{\varphi}_w = (\varphi_w^-, \varphi_w^+)$ collects the second components of the orthonormalized waveforms $\boldsymbol{\varphi}^{\mp}$. It can be demonstrated that $\boldsymbol{\varphi}_w$ is real-valued according to the mass ortho-normalization reported in the Appendix.

The general solution of the homogeneous equation pair (38a,b) at the lowest ϵ-order is the superposition of two real-valued, T_0-periodic and mutually orthogonal solution pairs (*generating solutions*). Specifically, the low-frequency generating solution $(\mathbf{q}_1^-, \mathbf{p}_1^-)$ and the high-frequency solution $(\mathbf{q}_1^+, \mathbf{p}_1^+)$ read

$$\mathbf{q}_1^{\mp} = A^{\mp}(T_1, T_2)\,\mathbf{a}_0^{\mp}\,\mathrm{e}^{\iota\omega^{\mp}T_0} + cc \qquad (42)$$
$$\mathbf{p}_1^{\mp} = \iota\omega^{\mp}A^{\mp}(T_1, T_2)\,\mathbf{a}_0^{\mp}\,\mathrm{e}^{\iota\omega^{\mp}T_0} + cc$$

where $\mathbf{a}_0^- = (1, 0)$ and $\mathbf{a}_0^+ = (0, 1)$ are the canonical base vectors of the two-by-two $\mathbf{q}$-space and $\mathbf{p}$-space, while cc stands for the complex conjugate of all the preceding terms. From the mathematical viewpoint, the variables $A^-(T_1, T_2)$ and $A^+(T_1, T_2)$ are complex-valued *unknown* amplitudes, depending on the slow time scales T_1 and T_2. According to the Multiple Scale Method, the high (second and third) order pairs of perturbation equations (38) have to be attacked to explicitly determine the functions $A^-(T_1, T_2)$ and $A^+(T_1, T_2)$.

From the physical viewpoint, the first-order asymptotic solution $\mathbf{q}_1^-$ describes the dominant (lowest order) component of the nonlinear elastic wave $\mathbf{u}_a = A^-(T_1, T_2)\,\boldsymbol{\varphi}^-\exp(\iota\omega^-T_0 - \iota\beta)$, freely propagating in space with the acoustic waveform $\boldsymbol{\varphi}^-(\beta)$ and *fast* mono-harmonically oscillating in time with the low-frequency $\omega^-(\beta)$ for a certain wavenumber β. Due to the quadratic and cubic nonlinearities, the unitary amplitude of the wave oscillations is *slowly* modulated by the *modulation amplitude $A^-(T_1, T_2)$*. Similarly, the first-order asymptotic solution $\mathbf{q}_1^+$ describes the dominant (lowest order) component of the nonlinear elastic wave $\mathbf{u}_a = A^+(T_1, T_2)\,\boldsymbol{\varphi}^+\exp(\iota\omega^+T_0 - \iota\beta)$, freely propagating in space with the optical waveform $\boldsymbol{\varphi}^+(\beta)$ and *fast* mono-harmonically oscillating in time with the high-frequency $\omega^+(\beta)$ for a certain wavenumber β. Due to the nonlinearities, the unitary amplitude of the wave oscillations is slowly modulated by the *modulation amplitude $A^+(T_1, T_2)$*.

Since the two nonlinear waves are expected to not interact with each other in the absence of internal resonances, it is convenient to study the two T_0-periodic solutions individually. Therefore, one *or* the other of the generating solutions (42) is considered, so that the superscripts $-$ and $+$ must be intended as mutually exclusive in the following. The considered oscillation frequency ω^- or ω^+ is referred to as the *leading frequency*. Substituting the mono-harmonic solution $(\mathbf{q}_1^-, \mathbf{p}_1^-)$ or $(\mathbf{q}_1^+, \mathbf{p}_1^+)$ in the ϵ^2-order equation pair (38c,d) yields

$$D_0\mathbf{p}_2 + \mathbf{\Omega}^2\mathbf{q}_2 = \mathbf{d}_2^{\mp}(\mathbf{q}_1^{\mp}, \mathbf{p}_1^{\mp}) \qquad (43)$$
$$D_0\mathbf{q}_2 - \mathbf{p}_2 = \mathbf{g}_2^{\mp}(\mathbf{q}_1^{\mp}, \mathbf{p}_1^{\mp})$$

11

where the two defects of homogeneity play the role of bi-harmonic forcing terms (with frequencies $\omega^\mp$ and $2\omega^\mp$) with unknown amplitudes

$$
\begin{aligned}
\mathbf{d}_2^\mp = &-\iota\omega^\mp D_1 A^\mp \, \mathbf{a}_0^\mp \, e^{\iota\omega^\mp T_0} + \\
&+ c_2(\omega^\mp)^2 A^\mp \bar{A}^\mp (\varphi_w^\mp)^2 \, \boldsymbol{\varphi}_w + \\
&+ 3c_2(\omega^\mp)^2 (A^\mp)^2 (\varphi_w^\mp)^2 \, \boldsymbol{\varphi}_w \, e^{2\iota\omega^\mp T_0} + cc
\end{aligned}
\tag{44}
$$

$$
\mathbf{g}_2^- = -D_1 A^\mp \, \mathbf{a}_0^\mp \, e^{\iota\omega^\mp T_0} + cc
$$

where the (T_1, T_2)-dependence of the amplitudes $A^\pm$ and $\bar{A}^\pm$ has been dropped for the sake of synthesis. The c_2-proportional contribution of the quadratic nonlinearities to the defect of homogeneity $\mathbf{d}_2^\pm$ can be recognized in (i) the T_0-independent term with amplitude $A^\pm \bar{A}^\pm$ and (ii) the T_0-dependent term with amplitude $(A^\mp)^2$, harmonically oscillating with double the leading frequency $\omega^\mp$.

Since at least one contribution in $\mathbf{d}_2^\pm$ and $\mathbf{g}_2^\pm$ oscillates with the leading frequency $\omega^\mp$, primary resonance with one or the other frequencies in the $\mathbf{\Omega}^2$-matrix occurs. Therefore, solvability conditions must be invoked to remove resonant (*secular*) terms, in order to preserve uniform perturbation expansions. The solvability condition can be imposed at each order by stating the adjoint linear homogeneous problem

$$
D_0 \tilde{\mathbf{p}} + \tilde{\mathbf{q}} = \mathbf{0}
\tag{45}
$$
$$
D_0 \tilde{\mathbf{q}} - \mathbf{\Omega}^2 \tilde{\mathbf{p}} = \mathbf{0}
$$

with the mutually exclusive T_0-periodicities $\tilde{\mathbf{q}}(0) = \tilde{\mathbf{q}}(T_0^\mp)$ and $\tilde{\mathbf{p}}(0) = \tilde{\mathbf{p}}(T_0^\mp)$ on one or the other linear periods $T_0^- = 2\pi/\omega^-$ and $T_0^+ = 2\pi/\omega^+$. Therefore, the solvability condition requires the orthogonality between the solutions of the adjoint problem

$$
\tilde{\mathbf{q}}^\mp = -\iota\omega^\mp B^\mp \mathbf{a}_0^\mp \, e^{\iota\omega^\mp T_0} + cc
\tag{46}
$$
$$
\tilde{\mathbf{p}}^\mp = B^\mp \mathbf{a}_0^\mp \, e^{\iota\omega^\mp T_0} + cc
$$

and the defects of homogeneity of the equation pair (43). The orthogonality can be stated as

$$
\int_0^{T_0^\mp} \left((\tilde{\mathbf{p}}^\mp)^\dagger \mathbf{g}_2^\mp + (\tilde{\mathbf{q}}^\mp)^\dagger \mathbf{d}_2^\mp \right) d\tau = 0.
\tag{47}
$$

Recalling that the product $(\mathbf{a}_0^\mp)^\top \mathbf{a}_0^\mp = 1$, the solvability condition requires that $D_1 A^\mp = 0$ and $D_1 \bar{A}^\mp = 0$. Consequently, the complex conjugate modulation amplitudes $A^\mp$ and $\bar{A}^\mp$ do not depend on the slow time-scale T_1. Imposing solvability, the particular solutions of the equation pair (43) read

$$
\begin{aligned}
\mathbf{q}_2^\mp = &A^\mp \bar{A}^\mp (\mathcal{K}_c^\mp \mathbf{a}_0^\mp + \mathcal{K}_o^\mp \mathbf{a}_0^\pm) + \\
&+ (A^\mp)^2 (Q_c^\mp \mathbf{a}_0^\mp + Q_o^\mp \mathbf{a}_0^\pm) \, e^{2\iota\omega^\mp T_0} + cc
\end{aligned}
\tag{48}
$$

$$
\mathbf{p}_2^\mp = 2\iota\omega^\mp (A^\mp)^2 (Q_c^\mp \mathbf{a}_0^\mp + Q_o^\mp \mathbf{a}_0^\pm) \, e^{2\iota\omega^\mp T_0} + cc
$$

where the modulation amplitudes must be understood to depend on the slowest time scale only, that is $A^\mp(T_2)$ and $\bar{A}^\mp(T_2)$. The relevant complex-valued quantities

$$
\mathcal{K}_c^\mp = c_2 \varphi_w^\mp (\varphi_w^\mp)^2, \quad \mathcal{K}_o^\mp = c_2 \frac{\varphi_w^\pm (\varphi_w^\mp)^2 (\omega^\mp)^2}{(\omega^\pm)^2}
\tag{49}
$$

$$
Q_c^\mp = -c_2 \varphi_w^\mp (\varphi_w^\mp)^2, \quad Q_o^\mp = 3c_2 \frac{\varphi_w^\pm (\varphi_w^\mp)^2 (\omega^\mp)^2}{(\omega^\pm)^2 - (2\omega^\mp)^2}
$$

multiply the contributions of the second order solution $\mathbf{q}_2^\mp$ that are *collinear* (direction $\mathbf{a}_0^\mp$ in the $\mathbf{q}$-space, subscript c) and *orthogonal* (direction $\mathbf{a}_0^\pm$ in the $\mathbf{q}$-space, subscript o) to the generating first order solution $\mathbf{q}_1^\mp$. Finally, the complementary solution of the equation pair (43) can be normalized to zero without loss of generality, because it is mono-harmonic (with frequency $\omega^\mp$) and collinear to the first-order solution $\mathbf{q}_1^\mp$.

Substituting the mono-harmonic first order solution $(\mathbf{q}_1^-, \mathbf{p}_1^-)$ or $(\mathbf{q}_1^+, \mathbf{p}_1^+)$ and the corresponding second order solution $(\mathbf{q}_2^-, \mathbf{p}_2^-)$ or $(\mathbf{q}_2^+, \mathbf{p}_2^+)$ in the ϵ^3-order equation pair (38e,f) gives

$$
D_0 \mathbf{p}_3 + \mathbf{\Omega}^2 \mathbf{q}_3 = \mathbf{d}_3^\mp (\mathbf{q}_1^\mp, \mathbf{p}_1^\mp, \mathbf{q}_2^\mp, \mathbf{p}_2^\mp)
\tag{50}
$$
$$
D_0 \mathbf{q}_3 - \mathbf{p}_3 = \mathbf{g}_3^\mp (\mathbf{q}_1^\mp, \mathbf{p}_1^\mp, \mathbf{q}_2^\mp, \mathbf{p}_2^\mp)
$$

where the two defects of homogeneity play the role of bi-harmonic forcing terms (with frequencies $\omega^\mp$ and $3\omega^\mp$) with unknown amplitudes

$$
\begin{aligned}
\mathbf{d}_3^\mp = &-\iota\omega^\mp D_2 A^\mp \, \mathbf{a}_0^\mp \, e^{\iota\omega^\mp T_0} + \\
&+ (\omega^\mp)^2 (A^\mp)^2 \bar{A}^\mp \mathcal{R}_3^\mp \boldsymbol{\varphi}_w \, e^{\iota\omega^\mp T_0} + \\
&+ (\omega^\mp)^2 (A^\mp)^3 \mathcal{C}_3^\mp \boldsymbol{\varphi}_w \, e^{3\iota\omega^\mp T_0} + cc
\end{aligned}
\tag{51}
$$

$$
\mathbf{g}_3^\mp = -D_2 A^\mp \, \mathbf{a}_0^\mp \, e^{\iota\omega^\mp T_0} + cc
$$

where the complex-valued coefficients multiplying the $(\omega^\mp)$-harmonic and $(3\omega^\mp)$-harmonic terms read

$$
\mathcal{R}_3^\mp = 2c_3(\varphi_w^\mp)^3 + 2c_2 \left(\mathcal{S}_c^\mp (\varphi_w^\mp)^2 + \mathcal{S}_o^\mp \varphi_w^\mp \varphi_w^\pm \right)
\tag{52}
$$
$$
\mathcal{C}_3^\mp = 2c_3(\varphi_w^\mp)^3 + 14c_2 \left(Q_c^\mp (\varphi_w^\mp)^2 + Q_o^\mp \varphi_w^\mp \varphi_w^\pm \right)
$$

and the auxiliary complex-valued quantities $\mathcal{S}_c^\mp = 2\mathcal{K}_c^\mp + 3Q_c^\mp$ and $\mathcal{S}_o^\mp = 2\mathcal{K}_o^\mp + 3Q_o^\mp$ have been also introduced.

Since at least one contribution in $\mathbf{d}_3^\pm$ and $\mathbf{g}_3^\pm$ oscillates with the leading frequency $\omega^\mp$, primary resonance with one or the other frequencies in the $\mathbf{\Omega}^2$-matrix occurs in equations (50). Therefore, a solvability condition must be imposed to preserve uniform perturbation expansion by removing resonant (*secular*) terms. Similarly to the second order, the solvability condition requires the orthogonality between the defects of homogeneity (51)

and the solutions of the adjoint problem (46). Therefore, imposing the orthogonality condition returns the *modulation equations* on the amplitude

$$D_2 A^\mp = -\tfrac{1}{2}\iota\omega^\mp \mathcal{R}_3^\mp \varphi_w^\mp (A^\mp)^2 \bar{A}^\mp \qquad (53)$$

while an analogous equation is found for the complex conjugate amplitude $\bar{A}^\mp$. Introducing the convenient polar form $A^\mp(T_2) = \tfrac{1}{2} a^\mp(T_2)\exp(\iota\,\gamma^\mp(T_2))$ and separating imaginary and real parts, equation (53) gives the coupled system of ordinary differential equations

$$D_2 a^\mp = 0, \qquad D_2\gamma^\mp = -\tfrac{1}{8}\mathcal{R}_3^\mp \varphi_w^\mp \omega^\mp (a^\mp)^2 \qquad (54)$$

The former equation states that the amplitudes $a^\mp$ are independent of the slow scale T_2, while integrating the latter equation establishes that the phase angles $\gamma^\mp$ linearly depend on the slow scale T_2 according to the function

$$\gamma^\mp(T_2) = \gamma_\circ^\mp - \tfrac{1}{8}\mathcal{R}_3^\mp \varphi_w^\mp \omega^\mp (a^\mp)^2 T_2 \qquad (55)$$

where $\gamma_\circ^\mp$ are constant phases assessable by imposing suited initial conditions. Therefore, the sought T_2-dependent complex-valued amplitudes $A^\pm$ finally read

$$A^\mp(T_2) = \tfrac{1}{2}\,a^\mp\, e^{\iota\,\gamma^\mp(T_2)} \qquad (56)$$

and, consequently, the first-order solutions $(\mathbf{q}_1^\mp, \mathbf{p}_1^\mp)$ and second order solutions $(\mathbf{q}_2^\mp, \mathbf{p}_2^\mp)$ are fully determined.

The third-order solutions $(\mathbf{q}_3^\mp, \mathbf{p}_3^\mp)$ can also be fully determined by imposing the solvability conditions (53) and solving the equation pair (50), yielding

$$\mathbf{q}_3^\mp = (A^\mp)^2 \bar{A}^\mp(\mathcal{R}_c^\mp \mathbf{a}_0^\mp + \mathcal{R}_o^\mp \mathbf{a}_0^\pm)\, e^{\iota\omega^\mp T_0} + \qquad (57)$$
$$+ (A^\mp)^3 (C_c^\mp \mathbf{a}_0^\mp + C_o^\mp \mathbf{a}_0^\pm)\, e^{3\iota\omega^\mp T_0} + cc$$

$$\mathbf{p}_3^\mp = -\iota\omega^\mp (A^\mp)^2 \bar{A}^\mp(\mathcal{R}_c^\mp \mathbf{a}_0^\mp - \mathcal{R}_o^\mp \mathbf{a}_0^\pm)\, e^{\iota\omega^\mp T_0} +$$
$$+ 3\iota\omega^\mp (A^\mp)^3 (C_c^\mp \mathbf{a}_0^\mp + C_o^\mp \mathbf{a}_0^\pm)\, e^{3\iota\omega^\mp T_0} + cc$$

where the relevant auxiliary quantities

$$\mathcal{R}_c^\mp = \tfrac{1}{4}\mathcal{R}_3^\mp \varphi_w^\mp, \quad \mathcal{R}_o^\mp = \mathcal{R}_3^\mp \frac{\varphi_w^\pm(\omega^\mp)^2}{(\omega^\pm)^2 - (\omega^\mp)^2} \qquad (58)$$

$$C_c^\mp = -\tfrac{1}{8}C_3^\mp \varphi_w^\mp, \quad C_o^\mp = C_3^\mp \frac{\varphi_w^\pm(\omega^\mp)^2}{(\omega^\pm)^2 - (3\omega^\mp)^2}$$

multiply the contributions of the third order solution $\mathbf{q}_3^\mp$ that are *collinear* (direction $\mathbf{a}_0^\mp$ in the $\mathbf{q}$-space, subscript c) and *orthogonal* (direction $\mathbf{a}_0^\pm$ in the $\mathbf{q}$-space, subscript o) to the generating first order solution $\mathbf{q}_1^\mp$. As with the second order, the complementary solution of the equation pair (50) can be normalized to zero without loss of generality.

As major consideration inherent to the perturbation theory, it must be remarked that the asymptotic consistency of the second-order solution (48) and the third order solution (54) is mathematically subordinated to the absence of wavefrequency ratios $\omega^+ : \omega^- \approx 1$ (one-to-one internal resonance or nearly resonance), $\omega^+ : \omega^- \approx 1/2$ or $\omega^+ : \omega^- \approx 1/3$ (one-to-two or one-to-three subharmonic internal resonances), as well as $\omega^+ : \omega^- \approx 2$ or $\omega^+ : \omega^- \approx 3$ (two-to-one or three-to-one superharmonic internal resonances). For a fixed wavenumber β, subharmonic resonances can certainly be excluded, due to the positiveness of the discriminant $\mathcal{J}_1(\beta)^2 - 4\mathcal{J}_2(\beta)$. Differently, superharmonic internal resonances may occur for particular combinations of the mechanical parameters. Since the adopted asymptotic strategy actually requires some specific mathematical refinements to account for internal resonance conditions [59, 68], the analyses in the following are limited to the general case of non-resonant metamaterials (namely featured by frequency ratios $\omega^+ - \omega^- = O(1)$, $\omega^+ - 2\omega^- = O(1)$ and $\omega^+ - 3\omega^- = O(1)$ for the selected wavenumber β).

3.3. Nonlinear dispersion properties

The asymptotic wave solution achieved by virtue of the method of multiple scales furnishes – as complementary and valuable outcome – the explicit parametric functions of the nonlinear dispersion properties, intended as the amplitude-dependent wavefrequencies $\varpi^\mp(a^\mp)$ and waveforms $\psi^\mp(a^\mp)$ of the time-periodic elastic waves freely propagating through the pantographic material.

Focusing first on the nonlinear wavefrequencies, the polar form (56) of the complex-valued amplitude $A^\pm$ can be expressed in the convenient form

$$A^\mp(\tau) = \tfrac{1}{2}\,a^\mp\, e^{\iota\left(\gamma_\circ^\mp + \epsilon^2 \omega_2^\mp \tau\right)} \qquad (59)$$

where $\omega_2^\mp = -\tfrac{1}{8}\mathcal{R}_3^\mp \varphi_w^\mp \omega^\mp (a^\mp)^2$ and the ordering relation $T_2 = \epsilon^2 \tau$ has been recalled to come back from the slow time-scale T_2 to the real time τ. The τ-dependent form of the amplitude $A^\mp(\tau)$ can properly be employed to express the first-order solution (42) in the form

$$\mathbf{q}_1^\mp(\tau) = \tfrac{1}{2}a^\mp \mathbf{a}_0^\mp\, e^{\iota\gamma_\circ^\mp + \iota\left(\omega^\mp + \epsilon^2 \omega_2^\mp\right)\tau} + cc \qquad (60)$$

which actually describes mono-harmonic τ-periodic oscillations. Indeed, the τ-multiplier $\omega^\mp + \epsilon^2 \omega_2^\mp$ can be mechanically interpreted as the *nonlinear frequencies* $\varpi^\mp$ of the τ-periodically oscillating waves, quadratically depending on the oscillation amplitude

$$\varpi^\mp = \omega^\mp + \epsilon^2 \omega_2^\mp = \omega^\mp - \tfrac{1}{8}\epsilon^2 \mathcal{R}_3^\mp \varphi_w^\mp \omega^\mp (a^\mp)^2. \qquad (61)$$

13

Since the second-order frequency correction can be expressed in the compact form $\omega_2^{\mp} = \kappa_2^{\mp}(a^{\mp})^2$, the relevant quadratic coefficient

$$\kappa_2^{\mp} = -\tfrac{1}{8}\mathcal{R}_3^{\mp}\varphi_w^{\mp}\omega^{\mp} = -\frac{\mathcal{Y}_{c3}^{\mp}}{4\omega^{\mp}} + \frac{(\mathcal{Y}_{c2}^{\mp})^2(3\omega^{\pm})^2}{\omega^{\mp}(3\omega^{\mp})^2(2\omega^{\pm})^2} + \quad (62)$$
$$+\frac{\mathcal{Y}_{c2}^{\mp}\mathcal{Y}_{o2}^{\pm}(3\omega^{\mp})^2}{\omega^{\mp}(3\omega^{\pm})^2(2\omega^{\pm})^2}\left(\frac{8(\omega^{\mp})^2-11(\omega^{\pm})^2}{(\omega^{\pm})^2-(2\omega^{\mp})^2}\right)$$

is referred to as the *effective nonlinearity coefficient*. Specifically, the $\kappa_2^{\mp}$-coefficient qualitatively characterizes the amplitude-dependent behavior of the nonlinear frequencies. A hardening behavior ($\kappa_2^{\mp} > 0$) or a softening behavior ($\kappa_2^{\mp} < 0$) can occur for different parameter combinations, depending on the linear frequencies and the linear waveforms that define the auxiliary quantities

$$\mathcal{Y}_{c3}^{\mp} = c_3(\omega^{\mp})^2(\varphi_w^{\mp})^4 \qquad (63)$$
$$\mathcal{Y}_{c2}^{\mp} = c_2(\omega^{\mp})^2(\varphi_w^{\mp})^3$$
$$\mathcal{Y}_{o2}^{\mp} = c_2(\omega^{\mp})^2(\varphi_w^{\mp})^2\varphi_w^{\pm}$$

It is worth remarking that the effective nonlinearity coefficient can even be null ($\kappa_2^{\mp} = 0$) for a locus $\mathcal{L}_\ell$ of particular parameter combinations, characterizing nonlinear metamaterials with amplitude-independent frequencies $\varpi^{\mp}$.

The nonlinear wavefrequencies $\varpi^{\mp}$ are illustrated in Figure 5, where the ratios $\varpi^{\mp}/\omega^{\mp}$ are reported versus increasing amplitudes $a^{\mp}$ for different mass ratios ϱ^2. The amplitude-dependent wavefrequency ratios are referred to the particular non-resonant metamaterial $\mathcal{N}$, characterized by the mechanical parameters $\alpha = \pi/5, \eta = 1$ at the wavenumbers $\beta = \pi/2$ (Figures 5a,b) and $\beta = 7/10\pi$ (Figure 5c). The corresponding linear frequencies are $\omega^- = 0.432$ and $\omega^+ = 0.963$ (for $\beta = \pi/2$) and $\omega^- = 0.576$ and $\omega^+ = 0.910$ (for $\beta = 7/10\pi$).

Looking at the nonlinear wavefrequencies $\varpi^{\mp}$ at the lower wavenumber $\beta = \pi/2$, the results highlight softening behaviour of both the nonlinear acoustic and optical frequencies, which is due to the dominant role played by the cubic (c_3-dependent) inertial nonlinearities over the quadratic (c_2-dependent) ones. The backbone curves obtainable for fixed ϱ^2-values (continuous mesh lines) show that the optical frequency decrement ϖ^+/ω^+ is greater than the acoustic frequency decrement ϖ^-/ω^- for increasing amplitudes. In fact, the same frequency reductions are reached for acoustic-to-optical amplitude ratios up to $a^-/a^+ = 5$. This finding can be justified by noting that the nonlinear optical waveform $\boldsymbol{\varphi}^+$ is strongly polarized on the configuration degree-of-freedom w (with *polarization factor* $\Lambda_w = 0.779$, see [21]), which is the only affected by nonlinearities. From the qualitative viewpoint, a certain mass ratio ϱ^2 can be found to determine a maximum in the nonlinear decrement of the optical frequency ϖ^+/ω^+ at large amplitudes a^+ (see for instance the iso-amplitude curves marked by the dashed mesh lines in Figure 5b). On the contrary, the nonlinear decrement of the acoustic frequency ϖ^-/ω^- monotonically increases for increasing mass ratios ϱ^2 (iso-amplitude dashed curves in Figure 5a).

Looking instead at the nonlinear acoustic frequency ϖ^- at the higher wavenumber $\beta = 7/10\pi$, it is interesting to note that the backbone behaviour is softening for small ϱ^2-values, while becomes hardening for large ϱ^2-values. This behaviour change occurs for a particular mass ratio $\varrho_\ell^2 \in \mathcal{L}_\ell$. For a fixed value $\varrho^2 = 1$, the regions of the (η, β)-parameter space corresponding to hardening acoustic behaviour (for several α-values in red-yellow scale) are non convex and internal to the locus $\mathcal{L}_\ell$ (black boundaries of the red-yellow scaled regions) illustrated in Figure 5d. In general, the hardening behaviour occurs for short wavelengths combined with large stiffness ratios. Furthermore, the hardening region reaches its maximum extent for α-values around $\pi/4$ and becomes thinner while moving towards larger β and lower η for higher values of the α-angles. For the sake of completeness, it can be remarked that the nonlinear optical frequency ϖ^+ at the higher wavenumber $\beta = 7/10\pi$ maintains instead a softening behaviour for all the ϱ^2-values.

Focusing on the nonlinear waveforms, the time-dependent and amplitude-dependent auxiliary variable $\theta^{\mp} = \gamma_o^{\mp} + (\omega^{\mp} + \epsilon^2\omega_2^{\mp})\tau$ can be introduced to express the first-order solution (42) in the trigonometric form

$$\mathbf{q}_1^{\mp} = a^{\mp}\mathbf{a}_0^{\mp}\cos\theta^{\mp} \qquad (64)$$
$$\mathbf{p}_1^{\mp} = -\omega^{\mp}a^{\mp}\mathbf{a}_0^{\mp}\sin\theta^{\mp}$$

Similarly, the second-order solutions (48) and third-order solutions (57) for displacements can also be expressed in the more convenient trigonometric form

$$\mathbf{q}_2^{\mp} = \tfrac{1}{2}(a^{\mp})^2(\mathcal{K}_c^{\mp}\mathbf{a}_0^{\mp} + \mathcal{K}_o^{\mp}\mathbf{a}_0^{\pm}) + \qquad (65)$$
$$+\tfrac{1}{2}(a^{\mp})^2(Q_c^{\mp}\mathbf{a}_0^{\mp} + Q_o^{\mp}\mathbf{a}_0^{\pm})\cos 2\theta^{\mp}$$

$$\mathbf{q}_3^{\mp} = \tfrac{1}{4}(a^{\mp})^3(\mathcal{R}_c^{\mp}\mathbf{a}_0^{\mp} + \mathcal{R}_o^{\mp}\mathbf{a}_0^{\pm})\cos\theta^{\mp} +$$
$$+\tfrac{1}{4}(a^{\mp})^3(C_c^{\mp}\mathbf{a}_0^{\mp} + C_o^{\mp}\mathbf{a}_0^{\pm})\cos 3\theta^{\mp}$$

where it is worth noting that, differently from the uncoupled first-order solutions $\mathbf{q}_1^{\mp}$, the higher-order solutions $\mathbf{q}_2^{\mp}$ and $\mathbf{q}_3^{\mp}$ are featured by nonlinear contributions from both the principal coordinates.

The ordered solutions (64) and (65) can be employed to reconstruct the trigonometric form of the principal
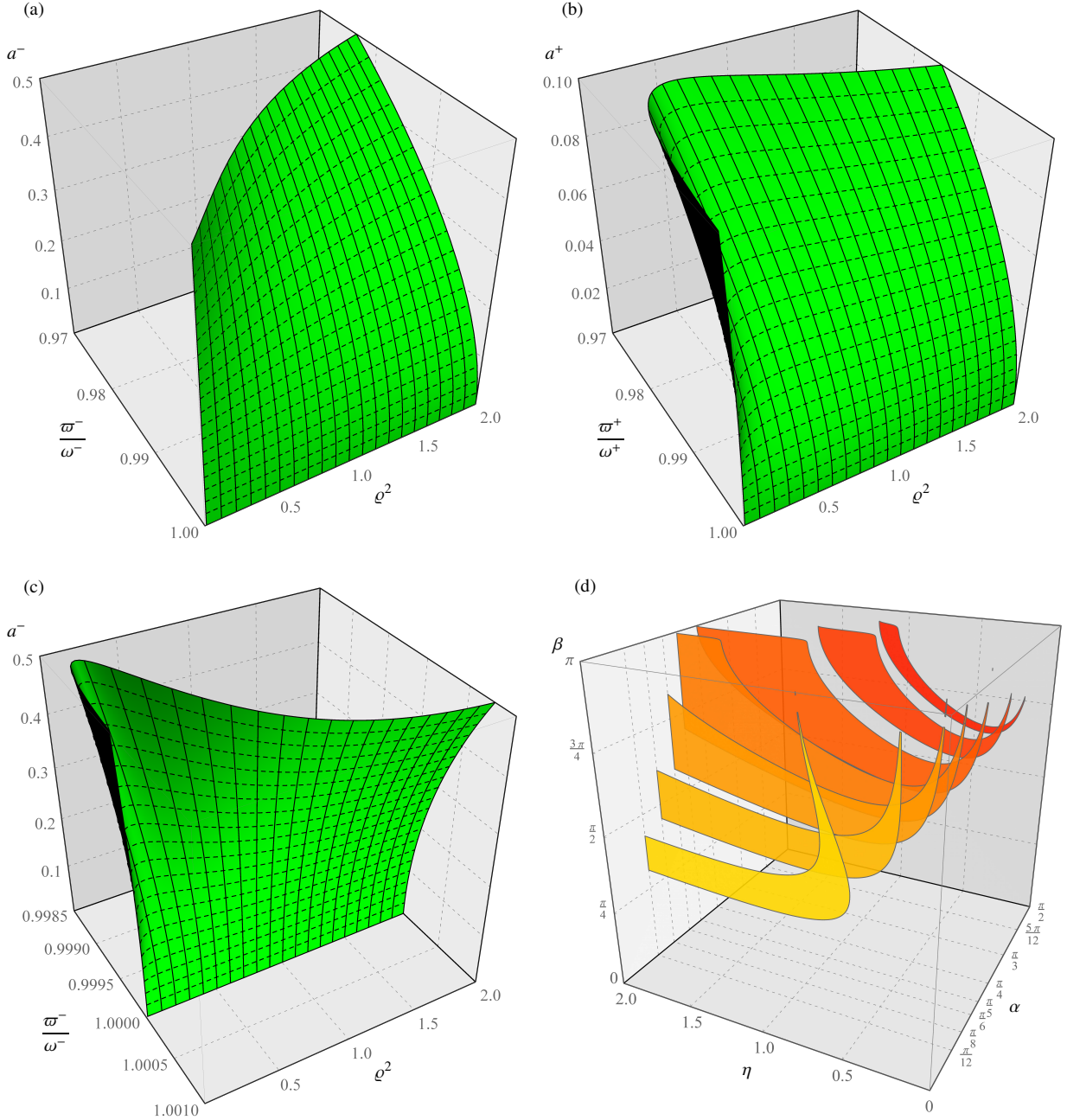
Figure 5: Nonlinear dispersion properties of the pantographic metamaterial $\mathcal{N}$: (a),(b) acoustic and optical nonlinear frequencies for $\beta = \pi/2$, (c) acoustic nonlinear frequency for $\beta = 7/10\pi$, (d) $\mathcal{L}_\ell$-bounded regions of acoustic hardening behaviour in the parametric space (α, η, β).

coordinate solution $\mathbf{q}^\mp = \epsilon\,\mathbf{q}_1^\mp + \epsilon^2\,\mathbf{q}_2^\mp + \epsilon^3\mathbf{q}_3^\mp + O(\epsilon^4)$. Therefore, the reconstructed solution allows also to determine a proper asymptotic approximation of the *nonlinear normal waveforms* $\boldsymbol{\psi}^-$ and $\boldsymbol{\psi}^+$. In analogy with the definition of nonlinear normal modes in structural dynamics [69, 70], the nonlinear normal waveforms can be intended as amplitude-dependent forms in the config-

urational coordinates, associated to the low-dimensional invariant manifolds $\mathcal{M}^-$ and $\mathcal{M}^+$ in the phase space of the principal coordinates. Specifically, the manifold $\mathcal{M}^-$ is fully determined in the space of the principal coordinates $\mathbf{q} = (q^-, q^+)$ once the second (*slave*) coordinate q^+ is analytically related to the first (*master*) coordinate q^- in the reconstructed solution $\mathbf{q}^-$. Conse-
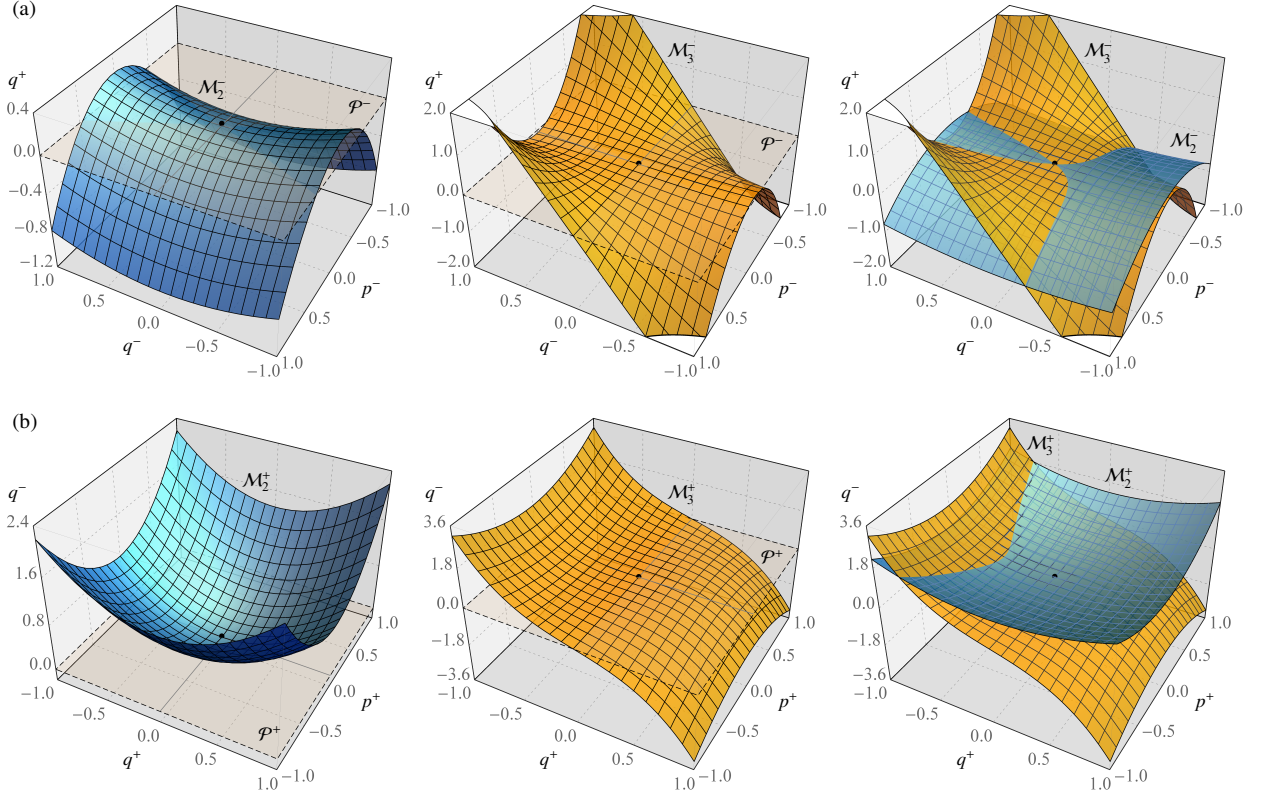
15

Figure 6: Nonlinear dispersion properties of the pantographic metamaterial $\mathcal{N}$: (a) second and third order acoustic manifolds $\mathcal{M}_2^-$ and $\mathcal{M}_3^-$, (b) second and third order optical manifolds $\mathcal{M}_2^+$ and $\mathcal{M}_3^+$.

quently, the invariant manifold $\mathcal{M}^-$ in the state space corresponds to the *nonlinear acoustic waveform* ψ^- in the space of the configurational coordinates $\mathbf{u}_a$. Similarly, the manifold $\mathcal{M}^+$ is fully determined in the space of the principal coordinates $\mathbf{q} = (q^-, q^+)$ once the first (*slave*) coordinate q^- is expressed in terms of the second (*master*) coordinate q^+ in the reconstructed solution $\mathbf{q}^+$. Consequently, the invariant manifold $\mathcal{M}^+$ in the state space corresponds to the *nonlinear optical waveform* ψ^+ in the space of the configurational coordinates $\mathbf{u}_a$.

From the operational viewpoint, equations (64) for $\mathbf{q}_1^-$ and $\mathbf{p}_1^-$ establish the first-order solutions $q^- = \epsilon a^- \cos \theta^-$ and $p^- = -\epsilon a^- \omega^- \sin \theta^-$. By substitution in the second-order and third-order solutions (65) for q^+, the manifold $\mathcal{M}^-$ is approximated by the principal coordinate relation

$$\mathcal{M}^- = \mathcal{M}_2^- + \mathcal{M}_3^- : \qquad (66)$$
$$q^+ = \mathcal{H}_2^+(q^-)^2 + \mathcal{G}_2^+(p^-)^2 + \mathcal{H}_3^+(q^-)^3 + \mathcal{G}_3^+ q^-(p^-)^2$$

which topologically corresponds to a cubic surface in

the three-dimensional phase space $\mathcal{F}^-$ spanned by the principal coordinates (q^-, p^-, q^+). The manifold $\mathcal{M}^-$ is locally tangent at the $\mathcal{F}^-$-origin to the manifold $\mathcal{M}_1^-$ of the linear waveform (defined by the equation $q^+ = 0$) corresponding to the phase plane $\mathcal{P}^-$ spanned by the co-ordinates (q^-, p^-). The higher-order terms of the manifold $\mathcal{M}^-$ can be referred to as the *second-order manifold* $\mathcal{M}_2^-$ and *third-order manifold* $\mathcal{M}_3^-$, for the sake of synthesis. Similarly, equations (64) for $\mathbf{q}_1^+$ and $\mathbf{p}_1^+$ establish the first-order solutions $q^+ = \epsilon a^+ \cos \theta^+$ and $p^+ = -\epsilon a^+ \omega^+ \sin \theta^+$. By substitution in the second-order and third-order solutions (65) for q^-, the manifold $\mathcal{M}^+$ is approximated by the principal coordinate relation

$$\mathcal{M}^+ = \mathcal{M}_2^+ + \mathcal{M}_3^+ : \qquad (67)$$
$$q^- = \mathcal{H}_2^-(q^+)^2 + \mathcal{G}_2^-(p^+)^2 + \mathcal{H}_3^-(q^+)^3 + \mathcal{G}_3^- q^+(p^+)^2$$

which topologically corresponds to a cubic surface in the three-dimensional phase space $\mathcal{F}^+$ spanned by the principal coordinates (q^+, p^+, q^-). The manifold $\mathcal{M}^+$ is

locally tangent at the $\mathcal{F}^+$-origin to the manifold $\mathcal{M}_1^+$ of the linear waveform (defined by the equation $q^- = 0$) corresponding to the phase plane $\mathcal{P}^+$ spanned by the coordinates (q^+, p^+). The higher-order terms of the manifold $\mathcal{M}^+$ can be referred to as the *second-order manifold $\mathcal{M}_2^+$* and *third-order manifold $\mathcal{M}_3^+$*, for the sake of synthesis. The auxiliary coefficients employed in the manifold approximation read

$$\mathcal{H}_2^{\pm} = \frac{\mathcal{K}_o^{\mp} + Q_o^{\mp}}{2}, \qquad \mathcal{G}_2^{\pm} = \frac{\mathcal{K}_o^{\mp} - Q_o^{\mp}}{2(\omega^{\mp})^2}, \qquad (68)$$
$$\mathcal{H}_3^{\pm} = \frac{\mathcal{R}_o^{\mp} + C_o^{\mp}}{4}, \qquad \mathcal{G}_3^{\pm} = \frac{\mathcal{R}_o^{\mp} - 3C_o^{\mp}}{4(\omega^{\mp})^2}$$

where $\mathcal{H}_2^{\pm}$ and $\mathcal{G}_2^{\pm}$ are the coefficients of the quadratic terms, sufficient to define the second-order manifolds $\mathcal{M}_2^{\mp}$, while $\mathcal{H}_3^{\pm}$ and $\mathcal{G}_3^{\pm}$ are the coefficients of the cubic terms, sufficient to define the third-order manifolds $\mathcal{M}_3^{\mp}$, in the phase-plane coordinates $(q^{\mp}, p^{\mp})$.

The second-order manifolds $\mathcal{M}_2^{\mp}$ (blue surfaces) and the third-order manifolds $\mathcal{M}_3^{\mp}$ (yellow surfaces) are reported in Figure 6 for the pantographic metamaterial $\mathcal{N}$ at the wavenumber $\beta = \pi/2$. The nonlinear acoustic manifolds $\mathcal{M}_2^-$ and $\mathcal{M}_3^-$ are portrayed in the three-dimensional phase space $\mathcal{F}^-$ (Figure 6a), while the nonlinear optical manifolds $\mathcal{M}_2^+$ and $\mathcal{M}_3^+$ are portrayed in the three-dimensional phase space $\mathcal{F}^+$ (Figure 6b). The black dots mark the tangency points between the manifolds and the invariant planes $\mathcal{P}^-$ and $\mathcal{P}^+$ associated with the corresponding linear waveforms (bounded by dashed lines). From the geometric viewpoint, the second-order acoustic manifold $\mathcal{M}_2^-$ is a hyperbolic paraboloid, whereas the second-order optical manifold $\mathcal{M}_2^+$ is an elliptic paraboloid. Furthermore, both the third-order acoustic and optical manifolds $\mathcal{M}_3^{\mp}$ show symmetry and anti-symmetry with respect to the planes $p^{\mp} = 0$ and $q^{\mp} = 0$, respectively. The topological difference between the shapes of the second- and third-order manifolds determine directions in the plane $\mathcal{P}^{\mp}$ with same-sign and opposite-sign contribution to the distortion of the linear manifold. From the quantitative viewpoint, the comparison between the manifolds show that the optical manifolds generally present larger principal curvatures with respect to the acoustic ones, corresponding to stronger amplitude-dependent distortions of the linear manifolds. This result can be justified by recalling that the nonlinear optical waveform $\boldsymbol{\varphi}^+$ is strongly polarized on the configuration degree-of-freedom w, which is the only affected by nonlinearities. It is worth remarking that the quantitative prevalence of the second-to-third order manifold is strongly dependent on the parameter combination and, even for the same metamaterial, on the wavenumber β.

Recalling the change of variables $\mathbf{u}_a = \boldsymbol{\Phi}\mathbf{q}$, the manifolds $\mathcal{M}^-$ and $\mathcal{M}^+$ can also be expressed in the space of the configuration variables $\mathbf{u}_a$ as

$$\mathcal{M}^- : \quad \mathbf{u}_a = q^- \boldsymbol{\varphi}^- + \left[\mathcal{H}_2^+(q^-)^2 + \mathcal{G}_2^+(p^-)^2 \right] \boldsymbol{\varphi}^+ + \quad (69)$$
$$+ \left[\mathcal{H}_3^+(q^-)^3 + \mathcal{G}_3^+ q^-(p^-)^2 \right] \boldsymbol{\varphi}^+$$

$$\mathcal{M}^+ : \quad \mathbf{u}_a = q^+ \boldsymbol{\varphi}^+ + \left[\mathcal{H}_2^-(q^+)^2 + \mathcal{G}_2^-(p^+)^2 \right] \boldsymbol{\varphi}^- +$$
$$+ \left[\mathcal{H}_3^-(q^+)^3 + \mathcal{G}_3^- q^+(p^+)^2 \right] \boldsymbol{\varphi}^-$$

Non-trivial initial conditions $q^-(\tau_\circ) = a$ and $p^-(\tau_\circ) = 0$ can be assigned into $\mathbf{u}_a$ for $\mathcal{M}^-$. Therefore, dividing by a to adopt a suited vector normalization, the third-order approximation of the nonlinear acoustic waveform is

$$\boldsymbol{\psi}^- = \boldsymbol{\varphi}^- + \left(a \mathcal{H}_2^+ + a^2 \mathcal{H}_3^+ \right) \boldsymbol{\varphi}^+ \qquad (70)$$

while, with analogous assignments of the initial conditions and normalization for $\mathcal{M}^+$, the third-order approximation of the second nonlinear optical waveform is

$$\boldsymbol{\psi}^+ = \boldsymbol{\varphi}^+ + \left(a \mathcal{H}_2^- + a^2 \mathcal{H}_3^- \right) \boldsymbol{\varphi}^- \qquad (71)$$

From the physical viewpoint, it can be remarked that the nonlinear waveforms $\boldsymbol{\psi}^{\mp}$ are conveniently expressed in the standard base of the orthogonal linear waveforms $\boldsymbol{\varphi}^{\mp}$. Specifically, the nonlinear acoustic waveform $\boldsymbol{\psi}^-$ is asymptotically approximated by linearly combining the linear acoustic waveform $\boldsymbol{\varphi}^-$ (dominant part) and the optical waveform $\boldsymbol{\varphi}^+$ (small part), scaled by an amplitude-dependent combination coefficient. On the contrary, the nonlinear optical waveform $\boldsymbol{\psi}^+$ is asymptotically approximated by linearly combining the linear optical waveform $\boldsymbol{\varphi}^+$ (dominant part) and the acoustic waveform $\boldsymbol{\varphi}^-$ (small part), scaled by an amplitude-dependent combination coefficient.

4. Numerical validation

An independent validation of the asymptotic approximations that analytically express the invariant manifolds can be provided by directly integrating the nonlinear equations of wave motion (see also [71, 72]). Therefore, the free undamped wave propagation is simulated by numerical solutions of the nonlinear equations (13), where the internal constraints $\mathbf{u}_p = -\mathbf{L}(\mathbf{L}^{\dagger}\mathbf{K}_{pp}\mathbf{L})^{-1}\mathbf{L}^{\dagger}\mathbf{D}\,\mathbf{z}$ and $\mathbf{f}_p = (\mathbf{I} - \mathbf{K}_{pp}\mathbf{L}(\mathbf{L}^{\dagger}\mathbf{K}_{pp}\mathbf{L})^{-1}\mathbf{L}^{\dagger})\mathbf{D}\,\mathbf{z}$ are imposed between passive and active variables and the changes of coordinates $\mathbf{u}_a = \boldsymbol{\Phi}\mathbf{q}$ and $\mathbf{v}_a = \boldsymbol{\Phi}\mathbf{p}$ are applied. Different sets of initial conditions (displacement $\mathbf{q}_0$ and velocity $\mathbf{p}_0$ at time $\tau = \tau_0$) are properly selected among the dynamic states belonging to the invariant manifolds $\mathcal{M}^{\mp}$, according to the asymptotic approximation.
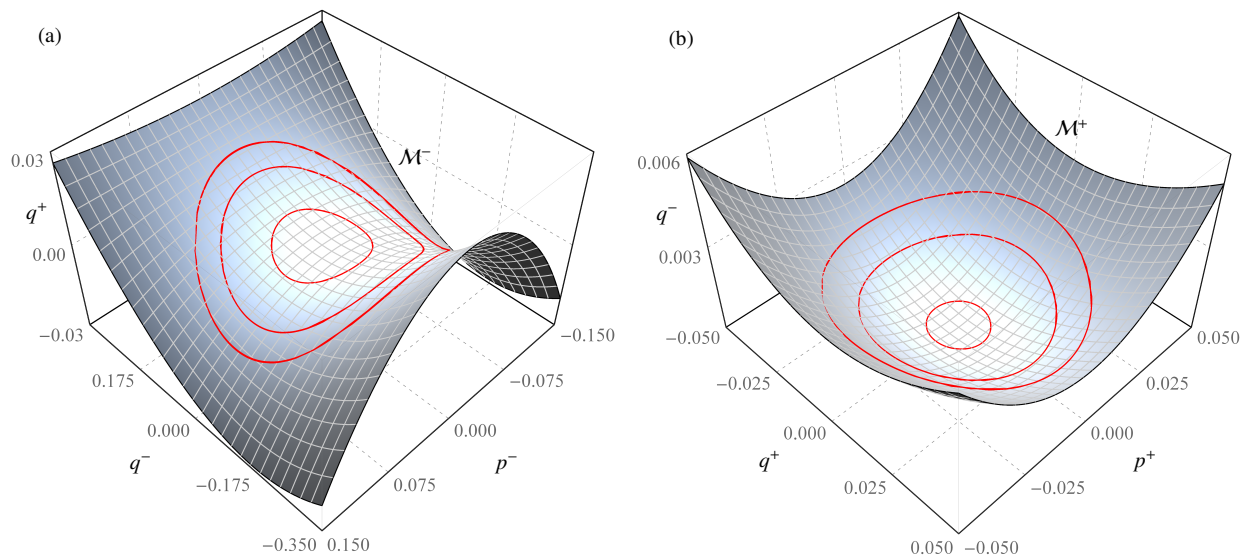
Figure 7: Comparison between numerical solutions (red curves) and analytical invariant manifolds associated with the nonlinear waveforms of the pantographic metamaterial $\mathcal{N}$: (a) orbits vs acoustic manifold $\mathcal{M}^-$, (b) orbits vs optical manifold $\mathcal{M}^+$.

As fundamental result, all the numerical integrations confirm the effectiveness of the asymptotic technique in determining the invariant nonlinear waveforms ψ^- and ψ^+ of the metamaterial. Indeed, the numerical time-histories of motion $\mathbf{q}(\tau)$ are systematically verified to describe periodic orbits in the range of small oscillation amplitudes. For the particular non-resonant metamaterial $\mathcal{N}$, Figure 7 illustrates three stable periodic responses corresponding to different initial conditions, superimposed to the invariant manifolds $\mathcal{M}^-$ and $\mathcal{M}^+$ defined by the coordinate relations (66) and (67). The

Table 1: Initial conditions (I.c.) for the numerical integration of the nonlinear equations governing the wave motion.

| Lattice (Manifold) | Coordinates | | I.c. |
	Master	Slave ($\times 10^{-4}$)	
$\mathcal{N}(\mathcal{M}^-)$	$(q_0^-, p_0^-) = (0.10, 0)$	$(q_0^+, p_0^+) = (20.369, 0)$	$\mathcal{I}_1$
	$(q_0^-, p_0^-) = (0.20, 0)$	$(q_0^+, p_0^+) = (78.447, 0)$	$\mathcal{I}_2$
	$(q_0^-, p_0^-) = (0.25, 0)$	$(q_0^+, p_0^+) = (120.208, 0)$	$\mathcal{I}_3$
$\mathcal{N}(\mathcal{M}^+)$	$(q_0^+, p_0^+) = (0.01, 0)$	$(q_0^-, p_0^-) = (0.866, 0)$	$\mathcal{I}_4$
	$(q_0^+, p_0^+) = (0.03, 0)$	$(q_0^-, p_0^-) = (7.459, 0)$	$\mathcal{I}_5$
	$(q_0^+, p_0^+) = (0.04, 0)$	$(q_0^-, p_0^-) = (12.964, 0)$	$\mathcal{I}_6$

growing $(\mathbf{q}_0, \mathbf{p}_0)$-values of the initial conditions for each set of numerical solutions are reported in Table 1, for the sake of reproducibility. It is worth noting that the initial conditions for the optical manifold $\mathcal{M}^+$ (conditions $\mathcal{I}_4$-$\mathcal{I}_6$) are significantly smaller (of about one order of magnitude with respect to the conditions $\mathcal{I}_1 - \mathcal{I}_3$ for the acoustic manifold $\mathcal{M}^-$), due to the larger nonlinearities affecting the principal coordinates in the associated equations. The satisfying agreement between the numerical results (red curves traced by ten periods of oscillation) and the analytical solutions (gray manifolds $\mathcal{M}^-$ and $\mathcal{M}^+$) can be appreciated by noting how all the periodic solutions sit on the manifold surfaces with fine qualitative and quantitative approximation. Consistently with the Multiple Scale Method, the asymptotic approximation tends to gradually degrade for larger initial conditions, which may violate the basic assumption of small oscillation amplitudes.

A further validating comparison is reported in Figure 8, where the numerical integrations (magenta circles) and the analytical solutions (black lines) are portrayed. Particularly, the analytical asymptotic solutions $\mathbf{q}^\mp$ are reconstructed as specified in Subsection 3.3 and truncated to the third order, after the reabsorption of the ϵ-parameter according to the Multiple Scale Method. Solutions corresponding to different initial conditions belonging to either the acoustic nonlinear manifold (Fig-
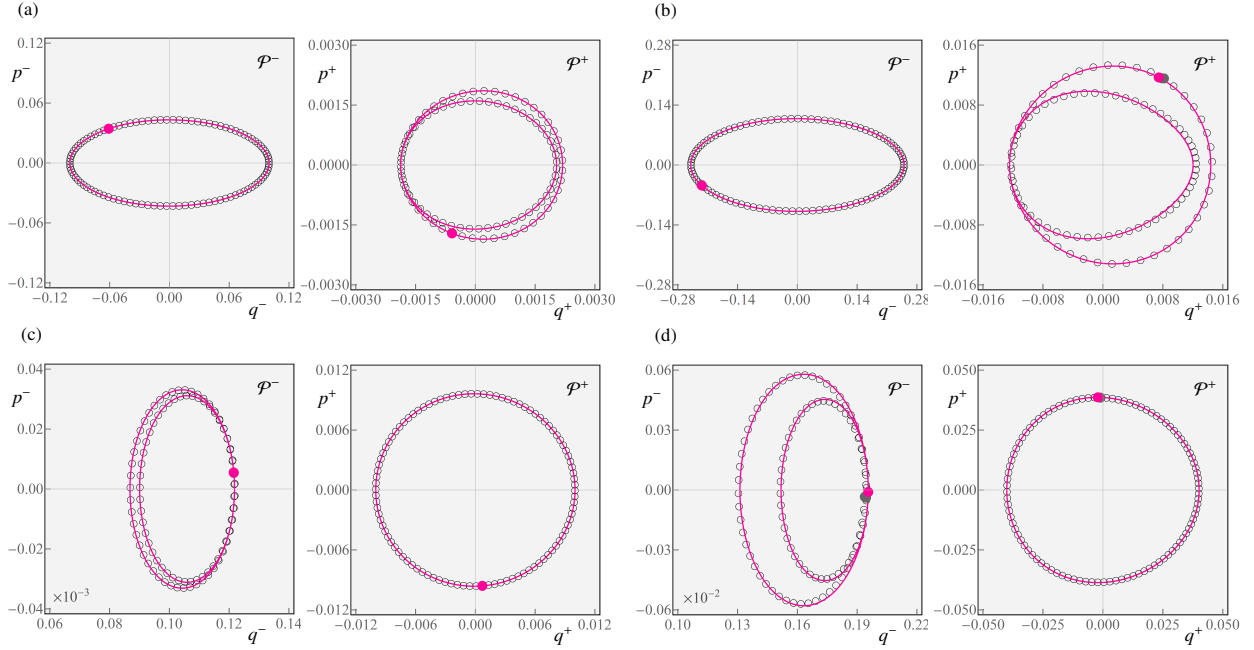
18

Figure 8: Comparison between numerical solutions (black circles) and analytical solutions (magenta lines) with detection of the Poincarè points (dots): (a),(b) periodic response with initial conditions $\mathcal{I}_1$ and $\mathcal{I}_3$ belonging to the nonlinear acoustic manifold $\mathcal{M}^-$; (c),(d) periodic response with initial conditions $\mathcal{I}_4$ and $\mathcal{I}_6$ belonging to the nonlinear optical manifold $\mathcal{M}^+$.

ures 8a,b) or the optical nonlinear manifold (Figure 8c,d) are considered and projected onto the phase planes $\mathcal{P}^-$ and $\mathcal{P}^+$. An excellent agreement can be appreciated for smaller ($\mathcal{I}_1$ and $\mathcal{I}_4$) and larger ($\mathcal{I}_3$ and $\mathcal{I}_6$) initial conditions. For both the manifolds, the master coordinates show a response dominated by the first-order harmonic component $\mathbf{q}_1^{\mp}$, whereas the slave coordinates show a response strongly characterized by the super-harmonic components of the higher-order solutions $\mathbf{q}_2^{\mp}$ and $\mathbf{q}_3^{\mp}$. This latter aspect is qualitatively recognizable by the double loop featuring the periodic orbits in the phase planes of the slave coordinates ($\mathcal{P}^+$ in Figures 8a,b, and $\mathcal{P}^-$ in Figures 8c,d). It is interesting to note the peculiar effect of the constant contribution in the second-order solutions $\mathbf{q}_2^{\mp}$, which causes the orbits to shift from the $\mathcal{P}^{\pm}$-origin, as more evident in the slave coordinate responses lying on the optical manifold $\mathcal{M}^+$. In the phase plane, the Poincaré points are also identified (magenta and black dots), by sampling the response at period $2\pi/\varpi^{\mp}$ [73]. The solution periodicity is confirmed by the single point representation of the Poincaré map in the planes $\mathcal{P}^{\mp}$, while the satisfying matching between analytical and numerical solutions is verified by the almost perfect coincidence between the respective points (closeness between magenta and black dots).

Conclusions

A one-dimensional microstructured lattice is proposed as minimal physical realization of a mechanical pantographic metamaterial with inertia amplification. The cellular microstructure is characterized by a straight deformable chain of principal atoms connected with pairs of eccentric secondary atoms, serving as tunable local inertia amplifiers. A discrete six degrees-of-freedom model is formulated to govern the undamped vibrations of the periodic tetra-atomic cell, according to a finite kinematic description. Imposing the axial indeformability of the interatomic connections (pantograph arms) allows the dimensional reduction to a condensed two-degrees-of-freedom model, fully described by a set of three independent nondimensional parameters (mass ratio, stiffness ratio, amplification angle). The rigid coupling generates quadratic and cubic inertial nonlinearities in the high-amplitude oscillation regime.

A general asymptotic approach, originally developed for nonlinear normal modes of structural systems, is employed to analytically determine the nonlinear dispersion properties of the pantographic metamaterial. Specifically, the Multiple Scale Method is adopted to reduce the governing equations of motion to an ordered hierarchy of linear ordinary differential problems, in

which the Floquet-Bloch theory can be applied to study the free propagation of harmonic waves. The methodological strategy can be considered quite general, and applicable to a class of mechanical metamaterials featured by similar periodic microstructures with local (intracellular) nonlinearities.

The linear dispersion properties are analytically determined by solving the wavenumber-dependent eigenproblem governing the lowest hierarchical order. The dispersion spectrum is composed by a low-frequency acoustic branch and a high-frequency optical branch. The band structure of the pantographic metamaterial is parametrically investigated by establishing invariant conditions for the pass and stop bands, according to the formal analogy with the Floquet theory for the stability of dynamical systems. As major theoretical achievement, the exact boundaries of the acoustic and optical pass bands, as well as the existence conditions and normalized amplitude of the stop band, are analytically assessed in the multi-dimensional parameter space. As functionally relevant finding, the centerfrequency of the stop band is found to significantly decrease with the relative mass of the inertia amplifiers, proving the suitability of the pantographic metamaterial to serve as low-frequency metafilter. Consequently, all the mechanical parameters can potentially work as design variables for spectral optimization purposes. For a certain parameter combination, the dispersion spectrum of real frequencies versus complex wavenumbers is discussed for different values of the mass of the inertia amplifiers. Propagation and attenuation branches are distinguished in the pass and stop bands, respectively.

Considering non-resonant lattices, the solution of the wavenumber-dependent problems governing the higher hierarchical orders allows to obtain the nonlinear dispersion properties. First, the nonlinear frequencies are determined as analytical functions of the parameters, quadratically depending on the oscillation amplitudes. In the general case, the acoustic and optical frequencies exhibit the typical softening behavior caused by dominant cubic nonlinearities in inertially nonlinear systems. However, particular regions corresponding to hardening acoustic frequencies can be identified in the parameter space. Second, each nonlinear waveform is analytically obtained as combination of the two linear waveforms. Differently from the nonlinear frequencies, the small combination coefficient is found to linearly and quadratically depend on the oscillation amplitude. Furthermore, the invariant manifolds associated with the nonlinear waveforms are parametrically determined both in the space of the principal coordinates and in the space of configurational variables.

A non-resonant lattice is selected to discuss and compare the nonlinear dispersion properties corresponding to different wavenumbers in the first Brillouin zone. The analytical solutions are successfully validated by running out numerical simulations of the amplitude-dependent free wave oscillations. Particularly, a satisfying agreement is systematically obtained from the direct comparison between the invariant manifolds predicted by the asymptotic strategy for the nonlinear waveforms and the stable periodic orbits described by the numerical solutions in the state space of the principal coordinates. Finally, an excellent matching between the analytical and numerical Poincaré maps is also achieved.

Acknowledgments

Appendix A. Hamiltonian action

The forth-order approximation of a nondimensional kinetic energy for the periodic tetra-atomic cell of the pantographic metamaterial reads

$$\mathcal{K} = \tfrac{1}{4}(2 + \varrho^2 + 4p_1^2\varrho^2)\dot{w}^2 + (1+\varrho^2)(\dot{u}^2 + \dot{u}\dot{w}) + \quad \text{(A.1)}$$
$$+ 4p_1 p_2 \varrho^2 w\dot{w}^2 + 4p_2(6p_1^3 + p_2)\varrho^2 w^2\dot{w}^2$$

whereas the nondimensional elastic potential energy takes the form

$$\mathcal{U} = u^2 + uw + \tfrac{1}{2}(1+\eta)w^2 + \tfrac{1}{2}(u_\ell^2 + u_r^2) + \quad \text{(A.2)}$$
$$- uu_\ell - uu_r - wu_r$$

Introducing the work done by the external forces $\mathcal{W} = f_\ell u_\ell + f_r u_r$, the Hamiltonian action between two instants of time t_1 and t_2 takes the integral expression

$$\mathcal{H} = \int_{t_1}^{t_2} (\mathcal{K} - \mathcal{V})\, dt \quad \text{(A.3)}$$

where $\mathcal{V} = \mathcal{U} - \mathcal{W}$ is the total potential energy. According to the Hamilton's principle, the Hamiltonian action can be imposed to be stationary to obtain the nonlinear equations of motion (6) and (9).

Appendix B. Linear dispersion properties

Appendix B.1. Matrices $\mathbf{R}_0$, $\mathbf{R}_1$, $\mathbf{R}_2$

The auxiliary matrices $\mathbf{R}_0$, $\mathbf{R}_1$, $\mathbf{R}_2$ necessary to define the eigenproblem (28) read

$$\mathbf{R}_0 = \begin{bmatrix} \mathbf{K}_{aa} - \mathbf{K}_{ap}^2 & \mathbf{O} \\ \mathbf{O} & \mathbf{M} \end{bmatrix}, \quad \mathbf{R}_1 = -\begin{bmatrix} \mathbf{K}_{ap}\mathbf{J}\mathbf{K}_{ap} & \mathbf{O} \\ \mathbf{O} & \mathbf{O} \end{bmatrix}, \tag{B.1}$$

$$\mathbf{R}_2 = -\begin{bmatrix} \mathbf{K}_{ap}\mathbf{J}^{\top}\mathbf{K}_{ap} & \mathbf{O} \\ \mathbf{O} & \mathbf{O} \end{bmatrix}, \quad \mathbf{J} = \begin{bmatrix} 0 & 1 \\ 0 & 0 \end{bmatrix}$$

Appendix B.2. Mass orthonormalization

The orthonormalized waveforms $\boldsymbol{\varphi}^{\mp}$ employed in the change of coordinates (37) are determined by multiplying the waveforms $\boldsymbol{\phi}^{\mp}$ by the mass-normalization factors

$$n^{\mp} = \frac{2\,|\omega^{\mp}|}{\phi_w^{\mp}\left((\boldsymbol{\phi}^{\mp})^{\dagger}\mathbf{K}\boldsymbol{\phi}^{\mp}\right)^{1/2}} = \frac{\sqrt{2}\,|\omega^{\mp}|}{\phi_w^{\mp}\left(\mathcal{U}_{\phi}^{\mp}\right)^{1/2}} \tag{B.2}$$

where $\phi_w^{\mp}$ is the second component of the waveform $\boldsymbol{\phi}^{\mp}$ and the positive quantity $\mathcal{U}_{\phi}^{\mp}$ is the elastic potential energy associated to the unitary-amplitude harmonic wave propagating with frequency $\omega^{\mp}$.

References

[1] L. Brillouin, Wave propagation in periodic structures: electric filters and crystal lattices, Courier Corporation, Mineola, New York, 2003.

[2] P. A. Deymier, Acoustic metamaterials and phononic crystals, Vol. 173, Springer Science & Business Media, 2013.

[3] V. Laude, Phononic crystals: artificial crystals for sonic, acoustic, and elastic waves, Vol. 26, Walter de Gruyter GmbH & Co KG, 2015.

[4] M.-H. Lu, L. Feng, Y.-F. Chen, Phononic crystals and acoustic metamaterials, Materials today 12 (12) (2009) 34–42.

[5] N. Fleck, V. Deshpande, M. Ashby, Micro-architectured materials: past, present and future, Proceedings of the Royal Society of London A: Mathematical, Physical and Engineering Sciences 466 (2121) (2010) 2495–2516.

[6] J.-H. Lee, J. P. Singer, E. L. Thomas, Micro-/nanostructured mechanical metamaterials, Advanced materials 24 (36) (2012) 4782–4810.

[7] M. I. Hussein, M. J. Leamy, M. Ruzzene, Dynamics of phononic materials and structures: Historical origins, recent progress, and future outlook, Applied Mechanics Reviews 66 (4) (2014) 040802.

[8] M. Kadic, G. W. Milton, M. van Hecke, M. Wegener, 3d metamaterials, Nature Reviews Physics 1 (2019) 198–210.

[9] A. Diaz, A. Haddow, L. Ma, Design of band-gap grid structures, Structural and Multidisciplinary Optimization 29 (6) (2005) 418–431.

[10] J. E. Cadman, S. Zhou, Y. Chen, Q. Li, On design of multifunctional microstructural materials, Journal of Materials Science 48 (1) (2013) 51–66.

[11] J. M. Manimala, C. Sun, Microstructural design studies for locally dissipative acoustic metamaterials, Journal of Applied Physics 115 (2) (2014) 023518.

[12] K. H. Matlack, M. Serra-Garcia, A. Palermo, S. D. Huber, C. Daraio, Designing perturbative metamaterials from discrete models, Nature materials 17 (4) (2018) 323–328.

[13] V. Settimi, P. Trovalusci, G. Rega, Dynamical properties of a composite microcracked bar based on a generalized continuum formulation, Continuum Mechanics and Thermodynamics 31 (6) (2019) 1627–1644.

[14] W. Wu, W. Hu, G. Qian, H. Liao, X. Xu, F. Berto, Mechanical design and multifunctional applications of chiral mechanical metamaterials: A review, Materials & Design (2019) 107950.

[15] A. Bacigalupo, G. Gnecco, M. Lepidi, L. Gambarotta, Machine-learning techniques for the optimal design of acoustic metamaterials, Journal of Optimization Theory and Applications 187 (3) (2020) 630–653.

[16] A. Bacigalupo, G. Gnecco, M. Lepidi, L. Gambarotta, Computational design of innovative mechanical metafilters via adaptive surrogate-based optimization, Computer Methods in Applied Mechanics and Engineering 375 (2021) 113623.

[17] F. Vadalá, A. Bacigalupo, M. Lepidi, L. Gambarotta, Free and forced wave propagation in beam lattice metamaterials with viscoelastic resonators, International Journal of Mechanical Sciences 193 (2020) 106129.

[18] J. S. Jensen, Phononic band gaps and vibrations in one-and two-dimensional mass–spring structures, Journal of Sound and Vibration 266 (5) (2003) 1053–1078.

[19] B. Liang, B. Yuan, J.-c. Cheng, Acoustic diode: Rectification of acoustic energy flux in one-dimensional systems, Physical review letters 103 (10) (2009) 104301.

[20] L. D'Alessandro, E. Belloni, R. Ardito, F. Braghin, A. Corigliano, Mechanical low-frequency filter via modes separation in 3d periodic structures, Applied Physics Letters 111 (23) (2017) 231902.

[21] A. Bacigalupo, M. Lepidi, Acoustic wave polarization and energy flow in periodic beam lattice materials, International Journal of Solids and Structures 147 (2018) 183–203.

[22] I. Grinberg, A. F. Vakakis, O. V. Gendelman, Acoustic diode: Wave non-reciprocity in nonlinearly coupled waveguides, Wave Motion 83 (2018) 49–66.

[23] Y.-F. Wang, Y.-Z. Wang, B. Wu, W. Chen, Y.-S. Wang, Tunable and active phononic crystals and metamaterials, Applied Mechanics Reviews 72 (4) (2020) 040801.

[24] L.-S. Wei, Y.-Z. Wang, Y.-S. Wang, Nonreciprocal transmission of nonlinear elastic wave metamaterials by incremental harmonic balance method, International Journal of Mechanical Sciences 173 (2020) 105433.

[25] X.-F. Li, X. Ni, L. Feng, M.-H. Lu, C. He, Y.-F. Chen, Tunable unidirectional sound propagation through a sonic-crystal-based acoustic diode, Physical review letters 106 (8) (2011) 084301.

[26] D. Bigoni, S. Guenneau, A. Movchan, M. Brun, Elastic metamaterials with inertial locally resonant structures: Application to lensing and localization, Physical Review B 87 (17) (2013) 174303.

[27] D. J. Colquitt, I. S. Jones, N. V. Movchan, A. B. Movchan, M. Brun, R. C. McPhedran, Making waves round a structured cloak: lattices, negative refraction and fringes, Proceedings of the Royal Society of London A 469 (2157) (2013) 20130218.

[28] S. A. Cummer, J. Christensen, A. Alù, Controlling sound with acoustic metamaterials, Nature Reviews Materials 1 (3) (2016) 16001.

[29] S. Guenneau, A. Movchan, G. Pétursson, S. A. Ramakrishna, Acoustic metamaterials for sound focusing and confinement, New Journal of physics 9 (11) (2007) 399.

[30] M. Ruzzene, F. Scarpa, F. Soranna, Wave beaming effects in two-dimensional cellular structures, Smart materials and structures 12 (3) (2003) 363–372.

[31] Y.-Z. Wang, F.-M. Li, Y.-S. Wang, Influences of active control on elastic wave propagation in a weakly nonlinear phononic crystal with a monoatomic lattice chain, International Journal of Mechanical Sciences 106 (2016) 357–362.

[32] Y. Chen, T. Li, F. Scarpa, L. Wang, Lattice metamaterials with mechanically tunable Poisson's ratio for vibration control, Physical Review Applied 7 (2) (2017) 024012.

[33] R. L. Lincoln, F. Scarpa, V. P. Ting, R. S. Trask, Multifunctional composites: A metamaterial perspective, Multifunctional Materials 2 (4) (2019) 043001.

[34] C. Yilmaz, G. Hulbert, Theory of phononic gaps induced by inertial amplification in finite structures, Physics Letters A 374 (34) (2010) 3576–3584.

[35] O. R. Bilal, M. I. Hussein, Trampoline metamaterial: Local resonance enhancement by springboards, Applied Physics Letters 103 (11) (2013) 111901.

[36] G. Ma, P. Sheng, Acoustic metamaterials: From local resonances to broad horizons, Science advances 2 (2) (2016) e1501595.

[37] J. Meaud, K. Che, Tuning elastic wave propagation in multistable architected materials, International Journal of Solids and Structures 122 (2017) 69–80.

[38] X. Xu, M. V. Barnhart, X. Fang, J. Wen, Y. Chen, G. Huang, A nonlinear dissipative elastic metamaterial for broadband wave mitigation, International Journal of Mechanical Sciences 164 (2019) 105159.

[39] N. M. Frandsen, O. R. Bilal, J. S. Jensen, M. I. Hussein, Inertial amplification of continuous structures: Large band gaps from small masses, Journal of Applied Physics 119 (12) (2016) 124902.

[40] M. Barys, J. S. Jensen, N. M. Frandsen, Efficient attenuation of beam vibrations by inertial amplification, European Journal of Mechanics-A/Solids 71 (2018) 245–257.

[41] S. Muhammad, S. Wang, F. Li, C. Zhang, Bandgap enhancement of periodic nonuniform metamaterial beams with inertial amplification mechanisms, Journal of Vibration and Control 26 (15–16) (2020) 1309–1318.

[42] O. Yuksel, C. Yilmaz, Realization of an ultrawide stop band in a 2-d elastic metamaterial with topologically optimized inertial amplification mechanisms, International Journal of Solids and Structures 203 (2020) 138–150.

[43] F. Romeo, M. Ruzzene, Wave propagation in linear and nonlinear periodic media: analysis and applications, Vol. 540, Springer Science & Business Media, 2013.

[44] W. Lacarbonara, Nonlinear structural mechanics: theory, dynamical phenomena and modeling, Springer, 2013.

[45] A. Pau, F. Vestroni, The role of material and geometric nonlinearities in acoustoelasticity, Wave Motion 86 (2019) 79–90.

[46] G. Rega, V. Settimi, S. Lenci, Chaos in one-dimensional structural mechanics, Nonlinear Dynamics 102 (2020) 785–834.

[47] A. F. Vakakis, M. E. King, Nonlinear wave transmission in a monocoupled elastic periodic system, The Journal of the Acoustical Society of America 98 (3) (1995) 1534–1546.

[48] B. S. Lazarov, J. S. Jensen, Low-frequency band gaps in chains with attached non-linear oscillators, International Journal of Non-Linear Mechanics 42 (10) (2007) 1186–1193.

[49] V. Rothos, A. Vakakis, Dynamic interactions of traveling waves propagating in a linear chain with an local essentially nonlinear attachment, Wave Motion 46 (3) (2009) 174–188.

[50] R. K. Narisetti, M. J. Leamy, M. Ruzzene, A perturbation approach for predicting wave propagation in one-dimensional nonlinear periodic structures, Journal of Vibration and Acoustics 132 (3) (2010) 031001.

[51] R. K. Narisetti, M. Ruzzene, M. J. Leamy, A perturbation approach for analyzing dispersion and group velocities in two-dimensional nonlinear periodic lattices, Journal of Vibration and Acoustics 133 (6) (2011) 061020.

[52] S. R. Panigrahi, B. F. Feeny, A. R. Diaz, Second-order perturbation analysis of low-amplitude traveling waves in a periodic chain with quadratic and cubic nonlinearity, Wave Motion 69 (2017) 1–15.

[53] S. R. Panigrahi, B. F. Feeny, A. R. Diaz, Wave–wave interactions in a periodic chain with quadratic nonlinearity, Wave Motion 69 (2017) 65–80.

[54] D. Hennig, G. P. Tsironis, Wave transmission in nonlinear lattices, Physics Reports 307 (5-6) (1999) 333–432.

[55] F. Romeo, G. Rega, Wave propagation properties in oscillatory chains with cubic nonlinearities via nonlinear map approach, Chaos, Solitons & Fractals 27 (3) (2006) 606–617.

[56] F. Romeo, G. Rega, Propagation properties of bi-coupled nonlinear oscillatory chains: analytical prediction and numerical validation, International Journal of Bifurcation and Chaos 18 (07) (2008) 1983–1998.

[57] X. Fang, J. Wen, J. Yin, D. Yu, Wave propagation in nonlinear metamaterial multi-atomic chains based on homotopy method, AIP Advances 6 (12) (2016) 121706.

[58] X. Fang, J. Wen, J. Yin, D. Yu, Y. Xiao, Broadband and tunable one-dimensional strongly nonlinear acoustic metamaterials: Theoretical study, Physical Review E 94 (5) (2016) 052206.

[59] W. Lacarbonara, R. Camillacci, Nonlinear normal modes of structural systems via asymptotic approach, International Journal of Solids and Structures 41 (20) (2004) 5565–5594.

[60] A. H. Nayfeh, Introduction to perturbation techniques, John Wiley & Sons, 2011.

[61] F. Romeo, A. Luongo, Invariant representation of propagation properties for bi-coupled periodic structures, Journal of Sound and Vibration 257 (5) (2002) 869–886.

[62] F. Romeo, A. Paolone, Wave propagation in three-coupled periodic structures, Journal of Sound and Vibration 301 (3-5) (2007) 635–648.

[63] G. Carta, M. Brun, Bloch–Floquet waves in flexural systems with continuous and discrete elements, Mechanics of Materials 87 (2015) 11–26.

[64] A. Krushynska, V. Kouznetsova, M. Geers, Visco-elastic effects on wave dispersion in three-phase acoustic metamaterials, Journal of the Mechanics and Physics of Solids 96 (2016) 29–47.

[65] M. Lewińska, V. Kouznetsova, J. Van Dommelen, A. Krushynska, M. Geers, The attenuation performance of locally resonant acoustic metamaterials based on generalised viscoelastic modelling, International Journal of Solids and Structures 126 (2017) 163–174.

[66] D. Mead, A general theory of harmonic wave propagation in linear periodic systems with multiple coupling, Journal of Sound and Vibration 27 (2) (1973) 235–260.

[67] J. C. Bronski, Z. Rapti, Modulational instability for nonlinear Schrödinger equations with a periodic potential, Dynamics of Partial Differential Equations 2 (4) (2005) 335–355.

[68] M. Lepidi, A. Bacigalupo, Wave propagation properties of one-dimensional acoustic metamaterials with nonlinear diatomic microstructure, Nonlinear Dynamics 98 (4) (2019) 2711–2735.

[69] S. Shaw, C. Pierre, Non-linear normal modes and invariant manifolds, Journal of Sound and Vibration 150 (1) (1991) 170–173.

[70] S. Shaw, C. Pierre, Normal modes for non-linear vibratory systems, Journal of Sound and Vibration 164 (1) (1993) 85–124.

[71] I. T. Georgiou, A. F. Vakakis, An invariant manifold approach for studying waves in a one-dimensional array of non-linear oscillators, International journal of non-linear mechanics 31 (6)

(1996) 871–886.

[72] F. Romeo, G. Rega, Periodic and localized solutions in chains of oscillators with softening or hardening cubic nonlinearity, Meccanica 50 (3) (2015) 721–730.

[73] H. Poincaré, Les méthodes nouvelles de la mécanique céleste, Vol. 1-3, Gauthier-Villars, 1899.